UNIVERSITY OF CALIFORNIA SAN DIEGO

The Forward and Reverse Genetics of Stomatal Gas Exchange in *Brachypodium distachyon*

A Thesis submitted in partial satisfaction of the requirements for the degree Master of Science

in

Biology

by

Morgana Andrée Sidhom

Committee in charge:

Professor Julian Schroeder, Chair
Professor Alisa Huffaker, Co-Chair
Professor Martin Yanofsky

2019

The Master's Thesis of Morgana Andrée Sidhom is approved, and it is acceptable in quality and form for publication on microfilm and electronically:

_____

_____

Co-Chair

_____

Chair

University of California San Diego

2019

TABLE OF CONTENTS

LIST OF FIGURES

LIST OF TABLES

ACKNOWLEDGEMENTS

Thank you to Paulo Ceciliato for allowing presentation of his Licor gas exchange analyses for candidates 1, 10, and 15 in this Master's thesis manuscript. Also thank you to Felipe Rangel who helped conduct the forward genetic screen.

ABSTRACT OF THE THESIS

The Forward and Reverse Genetics of Stomatal Gas Exchange in *Brachypodium distachyon*

by

Morgana Andrée Sidhom

Master of Science in Biology

University of California San Diego, 2019

Professor Julian Schroeder, Chair

Professor Alisa Huffaker, Co-Chair

Stomata are structures on the epidermis of leaves in plants that regulate exchange of gasses with the surrounding environment during photosynthesis and evapotranspiration. Because evapotranspiration serves to cool leaves, stomata also regulate canopy leaf temperatures. In grasses, stomata are made up of a central pore flanked by two guard cells and two subsidiary cells that help to regulate stomatal pore aperture. Subsidiary cells are hypothesized to promote more efficient responses to factors impacting stomatal aperture including atmospheric CO_2 levels and drought. To date, CO_2 signaling has not been investigated in grasses and more upstream transducers of the CO_2 mechanism remain to be identified. Using infrared thermography, a mutagenized population of *Brachypodium distachyon* was screened for potential defects in

stomatal responses.

The patterning of stomata also impacts overall gas exchange functionality in a plant. Stomatal development has been characterized in *Arabidopsis thaliana* and orthologues have been identified in members of the grass family including maize, rice, barley and *Brachypodium distachyon*. Transcription factors that are responsible for triggering changes in cell fate in the stomatal lineage are regulated by a kinase cascade that is initiated by accumulation and recognition of EPIDERMAL PATTERNING FACTORs (EPFs). EPFs have been shown to be processed and activated by members of the subtilase (SBT) family in Arabidopsis. The role of SBTs in stomatal development in Brachypodium has not been explored. Here, a reverse genetic screen for stomatal development in mutagenized *Brachypodium distachyon* lines endeavors to characterize the role of members of the SBT family in stomatal patterning.

Plants have evolved specialized structures on the epidermis of their leaves termed "stomata" to sense their environment and to allow for efficient direct responses, ensuring survival and adaptability (Bergmann, 2018; Chen et al., 2017; Rudall et al., 2017; Cotthem, 1970; Peterson et al., 2010). In dicot species such as *Arabidopsis thaliana*, the stomatal complex is made up of two kidney-shaped guard cells that enclose a pore. Guard cells sit above a cavity made up of photosynthetically active cells through which CO_2 and water vapor diffuse in and out during photosynthesis and evapotranspiration (Engineer et al., 2016). Gas exchange directly impacts leaf temperature as evapotranspiration is associated with lowering leaf temperatures in warmer climates (Hetherington & Woodward, 2003; Vrablova et al., 2017). In monocotyledonous species including grasses such as rice, wheat and the emerging crop model *Brachypodium distachyon* (Scholthof et al., 2018), stomata involve two separate cells termed "subsidiary" cells that participate in the dumbbell-shaped guard cells' gas exchange function (Bergmann 2018; Raissig et al. 2017; MacAllister et al. 2011). Subsidiary cells are thought to be ion sinks as well as hydraulic levers that counter guard cell turgidity (Bergmann 2018), allowing for a wider range of stomatal aperture and overall better transpiration efficiency (Chen et al., 2017). The subsidiary cell-less Brachypodium mutant *sic* identified by Raissig et al. (2017) shows reduced stomatal aperture in response to light. Further differences between dicot and monocot guard cells also include cell wall composition, allowing for greater variability in flexibility in monocot response dynamics (Bergmann, 2018).

Guard cells respond to abiotic and biotic factors by regulating stomatal apertures (Scavo et al., 2018). Drought, high CO_2, darkness and pathogen activation of the PAMP signaling pathway initiate stomatal closure while humidity, low CO_2, red and blue light trigger stomatal opening (Nilson & Assmann, 2007). The fungal toxin fusicoccin has been shown to override the

biotic signaling pathway by causing constitutive stomatal opening (Engineer et al., 2016), compromising plant immunity. Stomatal aperture regulation in response to low soil water content and humidity has been well characterized through genetic studies in the plant model *Arabidopsis thaliana* (Assmann & Jegla, 2016). Comparative functional genomic studies have shown that drought sensing pathways are well conserved across vascular plant species (Somyong et al., 2011; Ruszala et al., 2011; Chater et al., 2017; Chater et al., 2015; Munemasa et al., 2016). Drought is perceived through biosynthesis of the phytohormone abscisic acid (ABA) and subsequent activation of Ca^{2+} dependent and independent pathways that lead to efflux of osmolytes through anion channels including SLAC-1 (Xue et al., 2011) and concomitant loss of turgidity of the guard cells, initiating stomatal closure. Mutants in these ABA signaling components have been associated which lowered leaf temperatures and decreased drought tolerance (Merlot et al., 2002).

ABA signaling also participates in CO_2 perception but is not necessary for high CO_2 induced stomatal closure. In the Hsu et al. 2018 study, the ABA biosynthesis mutants *nced3*/*nced5*, positive regulators of ABA signaling PP2Cs *abi1* and *abi2*, and ABA receptor quadruple and hextuple mutants exhibited stomatal responsiveness to elevated atmospheric CO_2, albeit in a delayed manner.

CO_2 and ABA share molecular components in their signaling pathways. CO_2 is perceived through its conversion to bicarbonate by carbonic anhydrases (BETA CARBONIC ANHYDRASE 1 and BETA CARBONIC ANHYDRASE 4), which in turn binds to SLAC-1 anion channels (Zhang et al., 2018). Furthermore, OST1 was activated in response to bicarbonate, implicating it in high CO_2 mediated stomatal closure. Defects in CO_2 signaling have been observed to result in altered leaf temperatures than wild-type controls after exposure to

lower and higher atmospheric [CO_2] (Matrosova et al., 2015). Further studies are needed to identify other interactors that mediate stomatal opening and stomatal closure during CO_2-related responses (Zhang et al., 2018). CO_2 has also been shown to impact stomatal development (Engineer et al., 2014), although components responsible for linking CO_2 perception to stomatal development modules remain unclear.

Global levels of atmospheric CO_2 are rising (Keeling et al., 2011); further studies are needed to fully characterize the CO_2 signaling pathway to predict how elevated CO_2 conditions will impact crop productivity and yields. Cereal grains including wheat, barley, and rye make up a significant portion of agriculture; yet little has been reported on stomatal responses in these species (Vogel et al., 2009; Priest et al., 2014; Girin et al., 2018). Brachypodium, a relative of members of the cereal grains, has a smaller genome than its crop staple analogs, facilitating genetic studies (Benavente et al., 2013; Vogel et al., 2011). Studies in stomatal responses and development have been performed in the dicot species, Arabidopsis. However, dicots and monocots have been observed to diverge in several key aspects of plant processes and exhibit decreased gene synteny, making application of findings in dicot species to monocot species in the field difficult (Girin et al., 2018; Vogel et al., 2011). Exploration of the underlying mechanisms that govern plant development and fitness adaptability in Brachypodium can help improve crop tolerance in changing climates in the future.

I. Forward Genetic Screen in *Brachypodium distachyon*

1.1 Introduction

Mutants observed to be impaired in canopy leaf regulation have been identified to have defects in signalling components regulating stomatal movements. Arabidopsis mutants in OST1 were identified to be insensitive to ABA and CO_2 stimuli (Mustilli et al., 2002; Xue et al., 2011) and were observed to have a lower leaf temperature compared to wild type (Hashimoto et al., 2006). HT1 was shown to affect *ost1* phenotypes (Matrosova et al., 2015) as a negative regulator of stomatal closure. Mutants in HT1 display higher leaf temperatures than wild type at low CO_2 but still retain ABA responsiveness (Kim et al., 2010). Furthermore, the *gca2* (GROWTH CONTROLLED BY ABSCISIC ACID 2) mutant was shown to be insensitive to high CO_2-induced stomatal closure (Pei et al., 2000). ABA and CO_2 signalling exhibit pathway convergence (Assmann & Jegla, 2016; Hsu et al., 2018). Although ABA has been shown to potentiate the CO_2 response, it is not necessary to initiate CO_2–induced stomatal closure (Hsu et al., 2018). CO_2 is converted to HCO_3^- by BETA CARBONIC ANHYDRASE 2 and BETA CARBONIC ANHYDRASE 4 in guard cells (Hu et al., 2009). HCO_3 is thought to be the secondary messenger that transduces the CO_2 signal in a concentration-dependent manner (Zhang et al., 2018). Two CO_2 sensors that receive the bicarbonate signal have been identified to be SLAC-1 (Zhang et al., 2018) and RHC1 (Tian et al., 2015) SLAC-1 requires RHC1 repression of HT1 (Tian et al., 2015) for OST1 activation; further studies are needed to discover other bicarbonate interactors (Xue et al., 2011; Tian et al., 2015; Kim et al., 2010). Other sensors are thought to act upstream of the convergence point of ABA and CO_2 signalling pathways. Mutants identified to be CO_2 insensitive but responsive to exogenous ABA can lend further insight to delineate these two pathways and characterize more CO_2 sensors.

1.2 Results

1.2.1 Thermal imaging screening in Brachypodium for stomatal responses

Stomata are useful targets for improvement of crop production as their responses impact photosynthetic yield, drought tolerance, and overall water use efficiency. Criteria-specific forward genetic screens can provide a robust approach for identifying novel genes implicated in mechanisms that govern stomatal movements. *Brachypodium distachyon*, a forage grass that is a close relative of the wheat, barley, and rye family has a diploid genome with considerably less gene duplication than its crop staple counterparts (Brkljacic et al., 2011). Comparative genomic studies implementing Brachypodium as a starting point can help to elucidate key orthologues that are relevant to the growth of agricultural cultivars. A forward genetic screen was performed using an EMS mutagenized population of over 1000 M5 *Brachypodium distachyon* lines provided by the Joint Genome Institute (JGI). These lines are in the parental background BD21-3 which has been sequenced and published by JGI.

Thermography was used to identify lines within this library exhibiting altered canopy leaf temperatures compared to wild type, thus providing an indirect assessment of potential differences in stomatal conductance between mutant lines and wild type (Merlot et al., 2002; Ruiz et al., 2016; Leinonen et al., 2004; Benavente et al., 2013; Hashimoto et al., 2006). Each line was individually stored and screened in rounds of 45 lines with 5 replicate plants per line. Candidate lines exhibiting canopy leaf temperatures that differ from wild type are tested for impairments in regulation of stomatal aperture and stomatal development. Imaging takes places during the initial screening and a few days after, to verify that the phenotype is not due to changes in growth conditions. Lines exhibiting a consistent phenotype are ‘validated’ and ‘confirmed’, which involves reimaging lines after their initial isolation, and growing lines again within the same generation to determine

whether their phenotype can be re-observed, respectively. Finally, candidates undergo characterization of stomatal morphology and numbers, imaging after exposure to 900 ppm CO_2, followed by stomatal conductance analyses in both M5 and M6 generations (figure 1.1). These candidate lines are then sent in for whole genome sequencing analyses to identify the causative mutations. Candidate lines exhibiting identical phenotypes may be allelic and prepared for crossing as well as backcrossing to the parental line for reconfirmation of phenotypes in the progeny. Furthermore, once the mutated loci implicated in these lines' phenotypes is identified, CRSPR/Cas9 lines may be ordered and pursued.

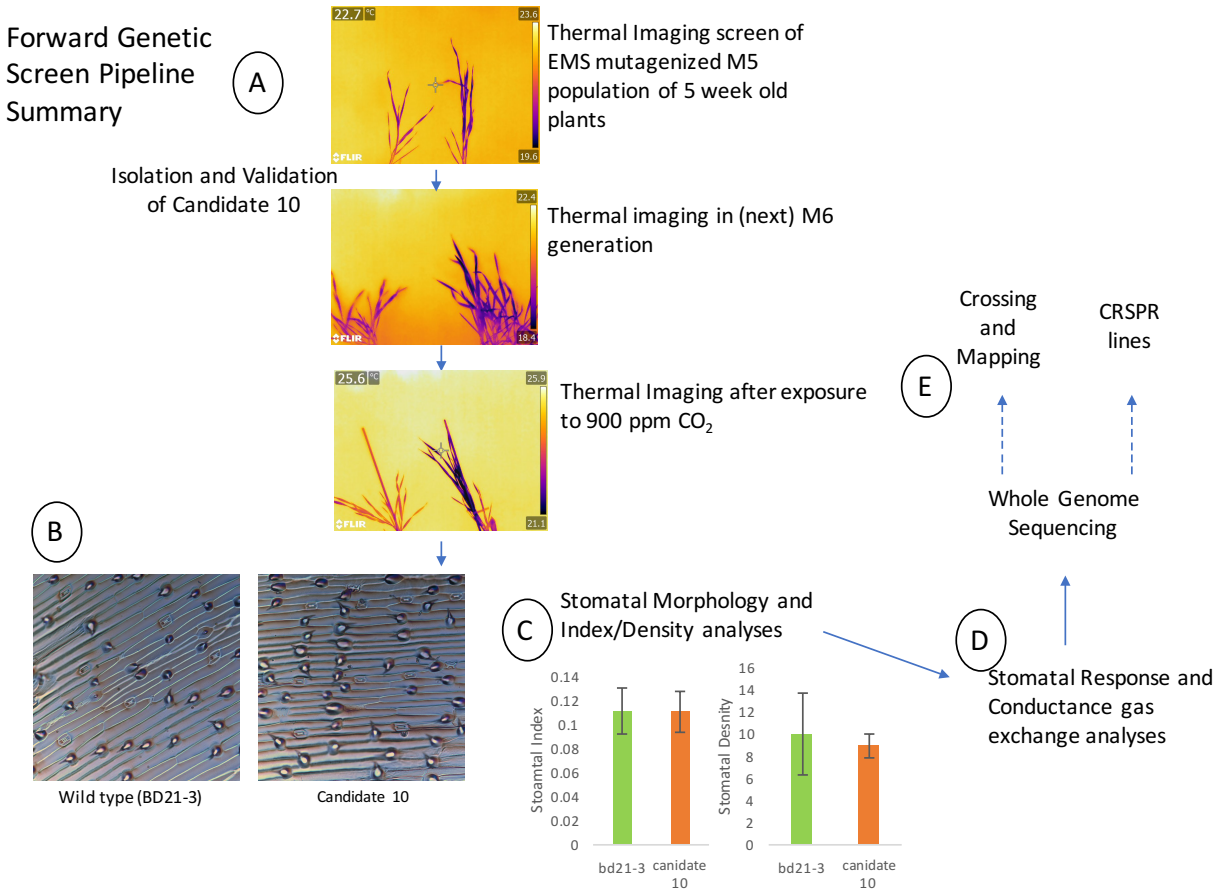

Figure 1.1: Forward genetic thermal imaging screen rationale and phenotyping experiments pipeline summary.

A-E describe each of the steps that are taken to characterize a mutant line isolated in a thermal imaging forward imaging screen for stomatal responses. **(A)** M5 EMS mutagenized lines are grown for 5 weeks and subjected to thermography for leaf temperature assessment. A candidate line that is identified to have altered canopy leaf temperatures compared to wild type at ambient CO_2 is regrown in the same generation (isolation) and the following generation (validation) and imaged again. Once the phenotype has been re-observed, candidate lines are imaged after exposure to high CO_2 for 3 hours and undergo **(B)** stomatal imaging experiments, **(C)** stomatal index/density distributions and morphology assessments, **(D)** stomatal gas exchange analyses. They are then **(E)** sent in for whole genome sequencing and entered into the pipeline for mapping of the causative mutation using crossing and targeted gene loci ablation (CRSPR/cas9) lines.

1.2.2 Identification of candidate lines with altered leaf temperatures compared to wild-type

Candidate lines identified to be impaired in the regulation of canopy leaf temperature may have a defect in stomatal response signalling components.

The screen first began by taking thermal images after exposing lines to high and low CO_2. Lower and higher than ambient atmospheric CO_2 concentrations have been shown to modulate stomatal apertures and movements in plants, thereby effecting macroscopic changes in canopy leaf temperatures (Negi et al, 2008**;** Engineer et al., 2016; Tian et al., 2015; Hashimoto et al., 2006; Wang et al., 2016; Wang et al., 2004). This screening protocol led to the identification of a mutant line termed "candidate 1" by Paulo Ceciliato that exhibits CO_2-specfic insensitivity that is ABA-independent. Candidate 1's phenotype is due to stomatal movement impairment, and not to aberrant stomatal development (figure 1.8; Paulo Ceciliato, unpublished). Its phenotype is not segregating and is observed in all the following M6, M7 and M8 generations that were tested (Paulo Ceciliato, unpublished data). This candidate line has also served as a tool of comparison for newly identified candidates in thermal imaging experiments performed after exposing lines to 900 ppm CO_2. (figure 1.4, panel B).

To increase the throughput of the screening, thermal imaging experiments were modified to take place at growth room conditions. Following this change in protocol, 20 other candidates with cooler leaf temperatures at ambient CO_2 compared to wild type were identified after screening 1350 M5 generation lines with Felipe Rangel (figure 1.2, figure 1.3, table 1.1). These candidates underwent specific phenotyping experiments assessing stomatal responses to high CO_2 (figure 1.5, 1.8, 1.9, 1.10) and stomatal morphology and densities (figure 1.6, 1.7).

Prior to screening, candidate lines were grown at 450 ppm, 40% humidity and in 16 light 8 h dark cycles for 5 weeks. Seeds were cold treated for 1 week prior to potting to ensure proper seed maturation and improved germination rates.

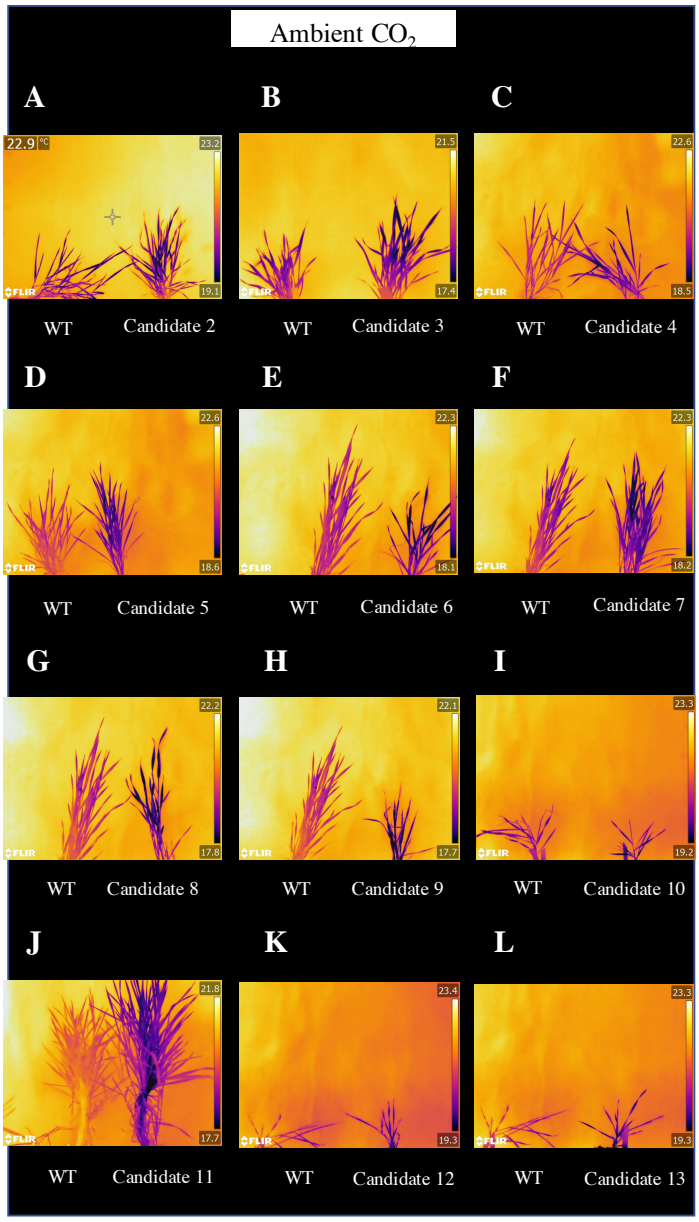

Figure 1.2: Representative images for thermal imaging screen at ambient CO_2 for candidates 2, 3, 4, 5, 6, 7, 8, 9, 10, 11, 12, 13 in M5 generation with cooler leaf temperatures compared to wild-type

Four-and-a-half to six-week old plants were grown and imaged at growth room CO_2 concentration and canopy leaf temperature was analysed by thermal imaging (WT-Bd21-3, left and candidates, right). At the time of experiment, the leaf temperatures of five independent plants per line were investigated alongside different wild type plants. Lighter colours (white-yellow-orange; in descending order) correspond to higher temperatures while darker colours (blue-purple-black; in descending order) correspond to lower temperatures. The candidate lines in A-L show cooler leaf temperatures. Note that the same wild type plant was used in panels E, F, G, H as imaging was performed in parallel for these candidates; panels K and L also include the same wild type plant.

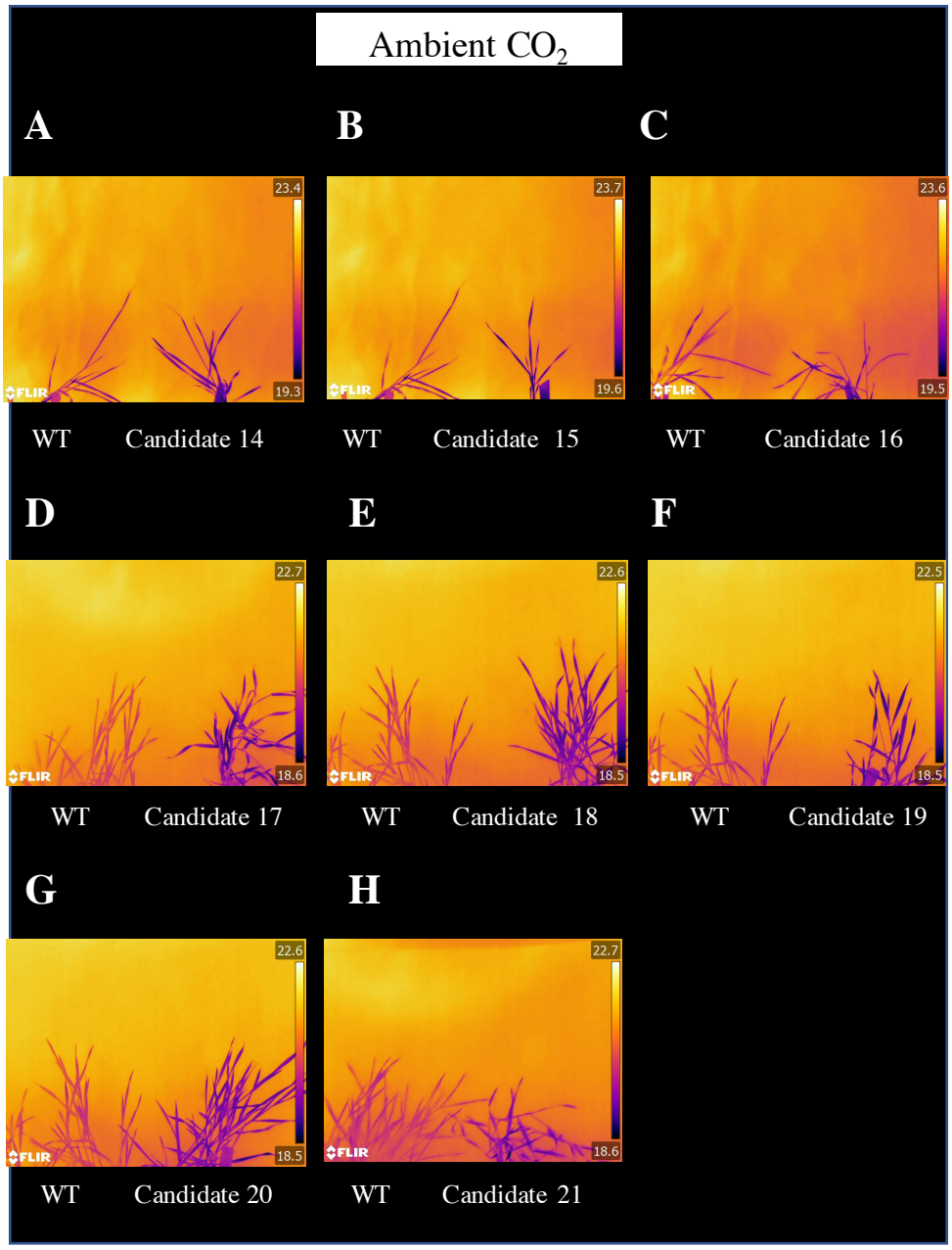

Figure 1.3: Representative images for thermal imaging screen at ambient CO_2 for candidates 14, 15, 16, 17, 18, 19, 20 and 21 in M5 generation

Four-and-a-half to six-week old plants were grown and imaged at growth room CO_2 concentration and canopy leaf temperature was analysed by thermal imaging (WT-Bd21-3, left and candidates, right). At the time of experiment, the leaf temperatures of five independent plants per line were investigated alongside different wild type plants. Lighter colours (white-yellow-orange; in descending order) correspond to higher temperatures while darker colours (blue-purple-black; in descending order) correspond to lower temperatures. The candidate lines in A-L show cooler leaf temperatures. Note that the same wild type plant was used in panels E, F, and G as imaging was performed in parallel for these candidates; panels A and B also include the same wild type plant.

1.2.3 Validation of candidate phenotypes in M6 generation

Candidates 2 to 21 were identified to have cooler leaf temperatures than wild type. Of these 20 candidates, 9 were tested and 9 were confirmed in the following M6 generation (figure 1.4). Images shown in figure 1.4 are from five to six-week-old plants.

According to Brkljacic et al., 2011, EMS mutagenesis approximately generates a mutation every 550 kilobases in *Brachypodium distachyon* (total of approximately 500 mutations for a 272 Mb genome) that segregate according to the expected Mendelian ratio in subsequent generations. Although M5 lines have a lower ratio of segregants, identification of segregants in the following generation can help to map the causative mutation. Figure 1.4 shows representative images taken for 9 candidates tested in the M6 generation following their isolation in the initial forward genetic screen.

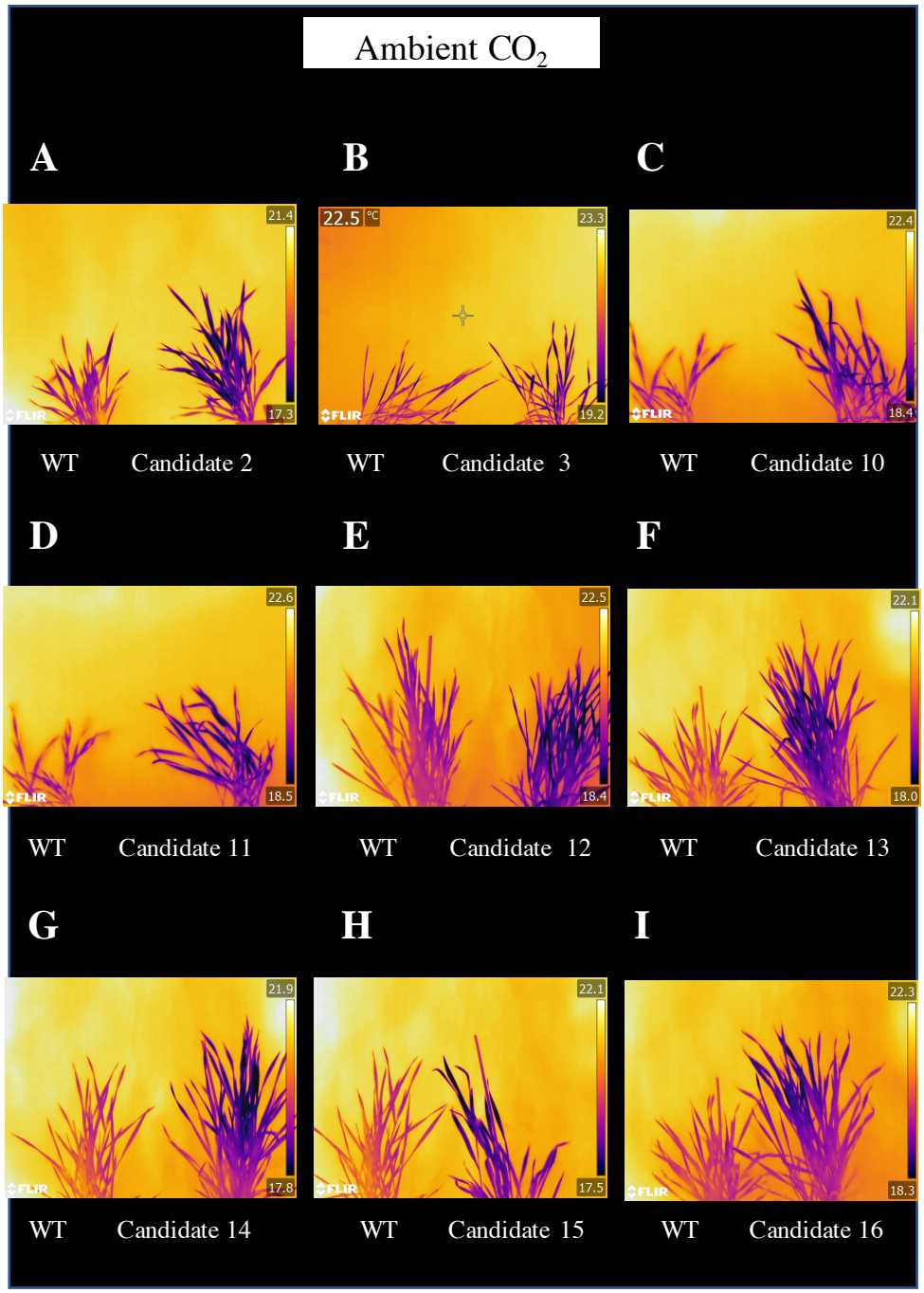

Figure 1.4: Representative images for thermal imaging screen at ambient CO_2 for candidates 2, 3, 10, 11, 12, 13, 14, 15, 16 in M6 generation

Five to six-week old plants were grown and imaged at growth room CO_2 concentration and canopy leaf temperature was analysed by thermal imaging (WT-Bd21-3, left and candidates, right). At the time of experiment, the leaf temperatures of five independent plants per line were investigated alongside different wild type plants. Lighter colours (white-yellow-orange; in descending order) correspond to higher temperatures while darker colours (blue-purple-black; in descending order) correspond to lower temperatures. The candidate lines in A-L show cooler leaf temperatures. Note that the same wild type plant was used in panels C and D, G and H, F and I as imaging was performed in parallel for these candidates.

1.2.4 Assessing CO_2 sensitivity using thermal imaging after high CO_2

High CO_2 causes a rise in C_i concentration, leading to stomatal closure (Santrucek et al., 2014). This decrease in stomatal apertures leads to increased leaf temperatures as leaves cannot perform evapotranspiration to cool their leaves. 16 lines were imaged either in M5 or M6 after exposure to 900 ppm CO_2 for 3 hours and 6 exhibited cooler leaf temperatures compared to wild type (figure 1.5). Aberrant leaf cooling in response to a stimulus that favours stomatal closure could be indicative of CO_2 insensitivity or another mechanism implicated in regulating leaf temperatures such as leaf cuticle wax biosynthesis (Jenks et al., 1995; Wang et al., 2004).

.

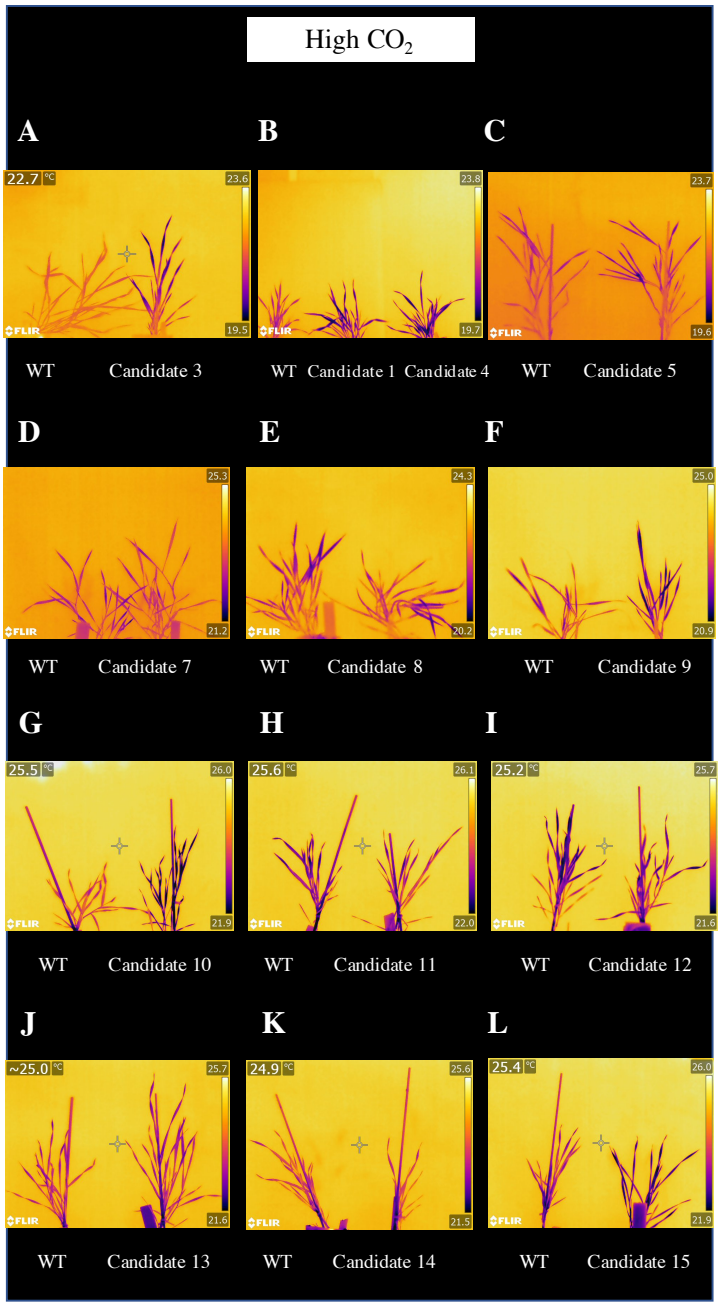

Figure 1.5: Representative thermal imaging at high CO_2 for candidates 3, 4, 5, 7, 8, 9, 10, 11, 12, 13, 14, 15

For this screening, a wild type was placed to the left of 5 independent plants for each of the candidate lines when images were captured. Lighter colours (white-yellow-orange; in descending order) correspond to higher temperatures while darker colours (blue-purple-black; in descending order) correspond to lower temperatures. Wild type (left) and the plants of the M6 generation of candidates 3, 4, 5, 7, 8, 9, 10, 11, 12, 13, 14, and 15 (right) were exposed to high CO_2 for 3 hours at 900 ppm along with wild type plants at the same developmental stage. Candidates 3, 4, 5, 9, 10, and 15 exhibited cooler leaf temperatures compared to wild type in response to elevated CO_2 while candidates 7, 8, 11, 13 and 14 show wild-type leaf temperatures. Note that panel B shows candidate 1 (which has been characterized for decreased CO_2 responsiveness in stomatal conductance assays) placed between wild type and candidate 4 for comparison.

1.2.5 Assessing stomatal morphology and numbers in candidate lines using Differential Interference Confocal (DIC) imaging

Grasses have laterally adjacent cells that make up the stomatal complex termed "subsidiary" cells that aid in stomatal responses. Mutants in subsidiary cell formation have been observed to have lower stomatal conductance in response to stimuli favouring stomatal-opening such as low CO_2 due to reduced stomatal aperture (Raissig et al., 2017). Increased stomatal densities have been observed to lower canopy leaf temperatures in *Arabidopsis thaliana* mutants in TMM (TOO MANY MOUTS), an EPF-ligand receptor that negatively regulates stomatal fate establishment, due to increased transpiration (Chaerle et al. 2005; Vrablova et al., 2017).

Candidates that have undergone stomatal index and density evaluations have so far not exhibited altered stomatal morphology and densities compared to wild type, indicating that their altered leaf temperatures are due to other mechanisms (figures 1.6 and 1.7). The fifth true leaf from five-week-old plants were selected. The abaxial side (Sugano et al., 2010; Abrash et al., 2018) of the centre of the leaf was peeled away, leaving behind the epidermal layer of the cells. The back of the epidermal layer of cells was imaged using 40x magnification and DIC microscopy (Leica CTR5000).

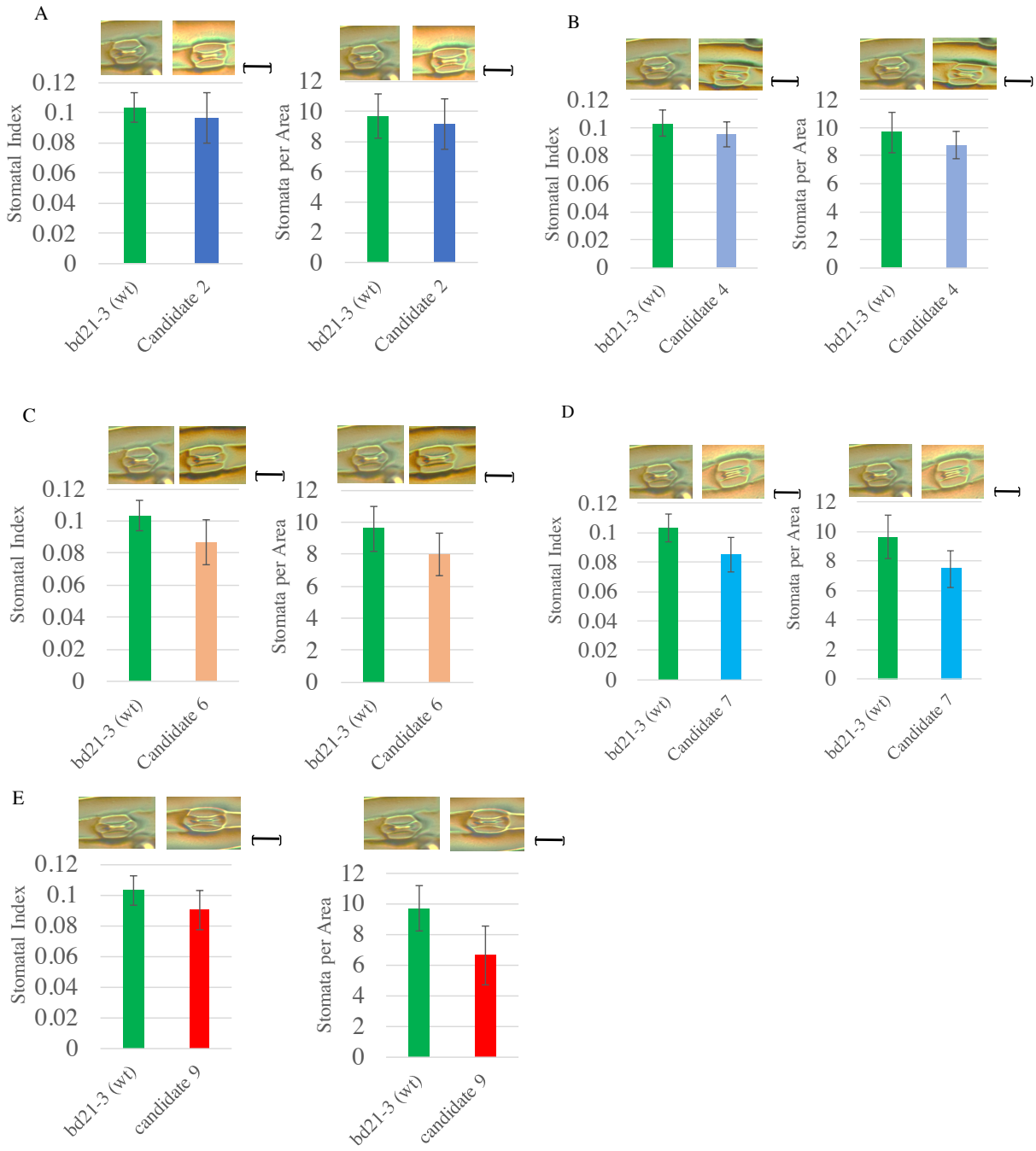

Figure 1.6: Representative leaf epidermis DIC imaging and stomatal analyses or candidates 2, 4, 6, 7, 9

Stomatal Index (left) and stomatal density (right) were calculated using 1 leaf, three images per leaf (fifth true leaf from three five-week old plants). Each bar represents the average of 3 plants per genotype and error bars represent SD. Leaves were imaged at 40x magnification. Microscopy images are included to show observed stomatal morphology. Note that the data for BD21-3 is the same in panels A-E as experiments for candidates 2, 4, 6, 7, and 9 were performed in parallel. The calibration bar for stomatal images depicts 20 μm.

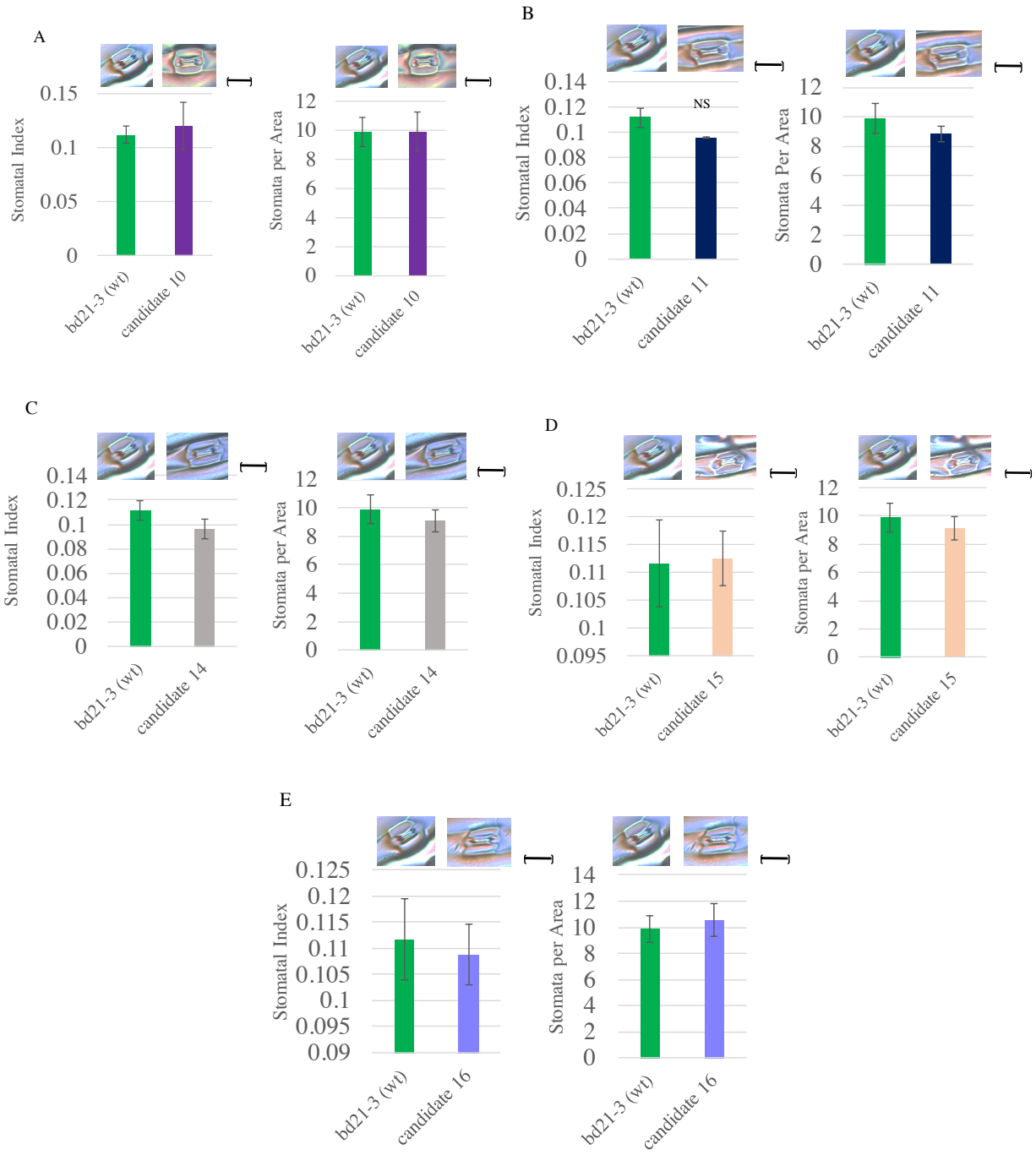

Figure 1.7: Representative leaf epidermis DIC imaging and stomatal analyses or candidates 10, 11, 14, 15, 16

Stomatal Index (left) and stomatal density (right) were calculated using 1 leaf, three images per leaf (fifth true leaf from three five-week old plants). Each bar represents the average of 3 plants per genotype and error bars represent SD. Leaves were imaged at 40x magnification. Microscopy images are included to show observed stomatal morphology. Note that the data for BD21-3 is the same in panels A-E as experiments for candidates 10, 11, 14, 15, and 16 were performed in parallel. The calibration bar for stomatal images depicts 20 μm.

1.2.6 Assessing CO_2 sensitivity using stomatal conductance analyses in response to altered atmospheric CO_2 concentrations (Paulo Ceciliato)

Stomatal conductance and stomatal responsiveness analyses can provide real-time understanding of a candidate line's ability to control stomatal aperture and provides a more direct assessment of stomatal function than thermal imaging (Hubbard et al., 2012).

The stomatal responsiveness of candidates 1, 15, and 10 were analyzed by Paulo Ceciliato. Candidate 1 showed a strongly insensitive high CO_2 response: while candidate 1 appears to undergo stomatal opening in response to low CO_2, candidate 1's stomatal conductance remained stagnant in response to high CO_2 stimuli (figure 1.8). This is in comparison to wild type's stomatal conductance which decreased with prolonged exposure to high CO_2. Candidate 15 also shows insensitivity to high CO_2 in addition to an inability to undergo low CO_2 induced stomatal opening (figure 1.9). Candidate 10 exhibits normal responsiveness to low CO_2 induced stomatal opening and initially demonstrates a decrease in stomatal conductance when exposed to high CO_2 (figure 1.10); however, candidate 10 appears to reopen its stomata during exposure to high CO_2, indicating a partial high CO_2 insensitivity. Candidate 10 remains to be assessed for ABA sensitivity; candidate 1 and candidate 15's CO_2 insensitivity is ABA-independent (table 1.1).

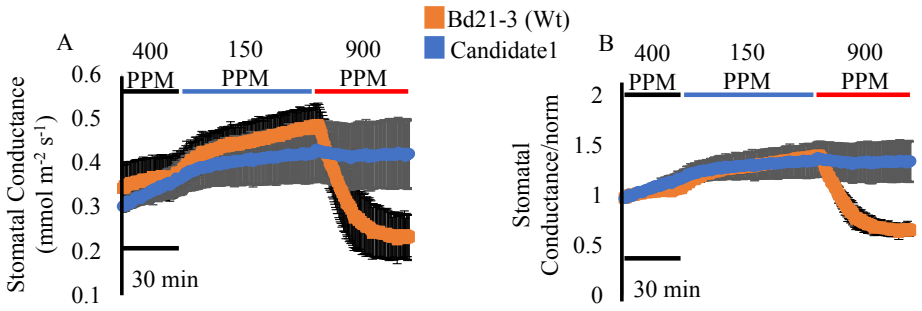

Figure 1.8: Candidate 1 is insensitive to [CO_2] elevation (**Paulo Ceciliato**)
A) The stomatal conductance of WT and candidate1 Brachypodium leaves was analyzed using a gas exchange analyzer. The graph shows average of n=3 ±SD experiments, four leaves per experiment (12 leaves total per genotype). **B)** The data from (A) were normalized to the average stomatal conductance of the 10 first minutes.

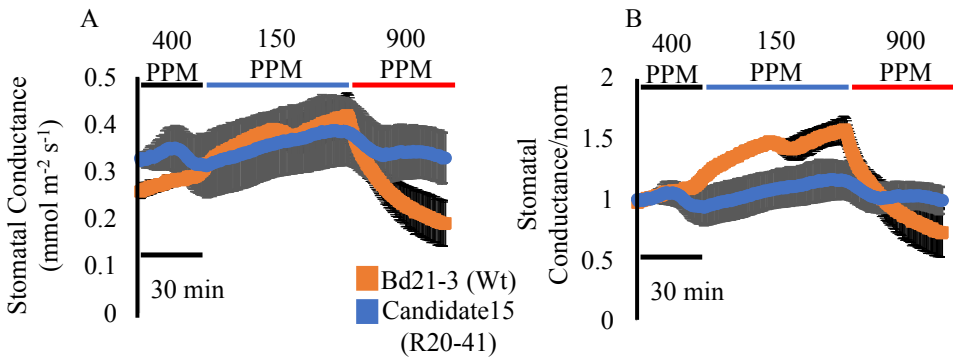

Figure 1.9: Candidate 15 shows insensitivity to [CO_2] shifts **(Paulo Ceciliato)**
A) The stomatal conductance of WT and candidate 15 Brachypodium leaves was analyzed using a gas exchange analyzer. The graph shows average of n=3 ±SD experiments, four leaves per experiment (12 leaves total per genotype). **B)** The data from (A) were normalized to the average stomatal conductance of the 10 first minutes.

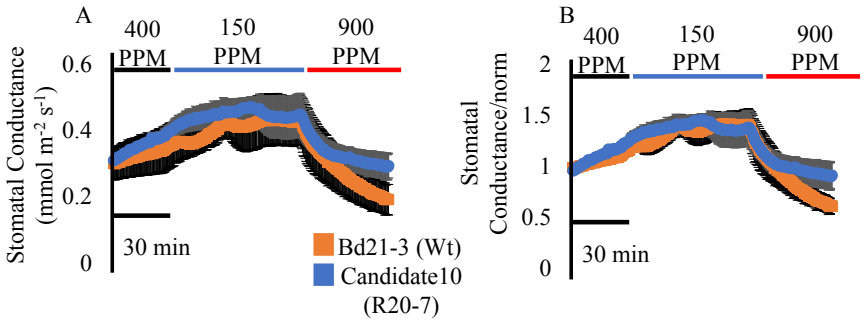

Figure 1.10: Candidate 10 is partially insensitive to high CO_2 (**Paulo Ceciliato**)
Candidate 10 shows responses to [CO_2] shifts and normal stomatal development. **A)** The stomatal conductance of WT and candidate 10 Brachypodium leaves was analyzed using a gas exchange analyzer. The graph shows average of n=3 ±SD experiments, four leaves per experiment (12 leaves total per genotype). **B)** The data from (A) were normalized to the average stomatal conductance of the 10 first minutes.

Table 1.1: Summary table of phenotyping experiments for candidate lines, continued.
Mutant candidates and the status of the screen performed with Felipe Rangel and Paulo Ceciliato. In total, 12 of 19 mutants were confirmed in screening M6 generation plants and the remaining 9 of the initial 21 putative mutants are being tested in the M6 generation. Thus, presently a total of 21 lines (12 + 9) are being investigated.
**Genome DNA sent for WGS=Whole Genome Sequencing.

Re-tested Candidates in M5 generation: Colder than Wild Type at Ambient CO_2	Confirmed in M6 generation	Stomatal Density Imaging	Results on Stomatal Density	Results of Thermal imaging under high CO_2	Insensitive to CO_2	LiCOR Gas Exchange (ABA)	WGS
Candidate 1	x	x	WT-like	colder	yes	x	x
R6-33 (candidate 2)	x	x	WT-like	colder	no	NA	x**
R4-45 (candidate 3)	x	x	WT-like	colder	no	NA	x**
R5-18 (candidate 4)	x	x	WT-like	colder	no	NA	x**
R6-18 (candidate 5)	x	x	WT-like	colder			x**
R21-29 (candidate 6)		x	WT-like	WT-like			
R21-32 (candidate 7)		x	WT-like	WT-like			
R21-30 (candidate 8)		x	WT-like	WT-like			
R21-33 (candidate 9)		x	WT-like	colder	no	NA	

Table 1.1 continued

Re-tested Candidates in M5 generation: Colder than Wild Type at Ambient CO_2	Confirmed in M6 generation	Stomatal Density Imaging	Results on Stomatal Density	Results of Thermal imaging under high CO_2	Insensitive to CO_2	LiCOR Gas Exchange (ABA)	WGS
R20-7 (candidate 10)	x	x	WT-like	colder	partial	ongoing	
R20-8 (candidate 11)	x	x	WT-like	WT-like	no	NA	
R20-18 (candidate 12)	x	x	WT-like	WT-like	no	NA	
R20-38 (candidate 13)	x	x	WT-like	WT-like	no	NA	x**
R20-40 (candidate 14)	x	x	WT-like	WT-like	no	NA	x**
R20-41 (candidate 15)	x	x	WT-like	colder	yes	x	x
R20-43 (candidate 16)	x	x	WT-like	colder	no	NA	x**
R30-4 (candidate 17)							

Table 1.1 continued

Re-tested Candidates in M5 generation: Colder than Wild Type at Ambient CO_2	Confirmed in M6 generation	Stomatal Density Imaging	Results on Stomatal Density	Results of Thermal imaging under high CO_2	Insensitive to CO_2	LiCOR Gas Exchange (ABA)	WGS
R31-1 (candidate 18)							
R31-34 (candidate 19)							
R31-5 (candidate 20)							
R30-7 (candidate 21)							

1.3 Discussion

Screening a large population of mutants has proven to have the potential for characterizing new genes and their roles in the regulation of stomatal movements. Measuring leaf temperature can serve as a pilot assessment of the functionality of stomatal mechanisms and programs (Merlot et al., 2002; Vrablova et al., 2017). Thermal imaging has been instrumental to the isolation of 21 candidates with cooler leaf temperatures compared to wild type at ambient CO_2. Stomatal morphology and density analyses showed that these mutants did not have an impairment in stomatal development. Two mutants identified to be CO_2 insensitive exhibited ABA responsiveness, implicating a defect in a CO_2-specific transducer of the response. One mutant that was identified to be partially insensitive to changes in CO_2 concentrations still remains to be characterized for ABA response dynamics. Further stomatal conductance analyses are needed to make conclusive remarks on the CO_2 responsiveness of candidates imaged to be cooler than wild type after exposure to elevated CO_2. Mutants putatively exhibiting an intact CO_2 response (candidates 13, 14, 16; table 1.1) may have a defect in other components impacting leaf temperature not directly related to CO_2 sensing or stomatal patterning such as cuticle wax biosynthesis (Jenks et al., 1995; Yang et al., 2011).

The CO_2 and ABA signaling pathways interact to coordinate stomatal responses and have been implicated in controlling leaf temperature (Merlot et al., 2002). Mutations in several ABA signaling components have been found to be concomitant with an inhibited CO_2 response (Chater et al., 2015). Mutants identified in Arabidopsis that exhibit ABA-dependent CO_2 insensitivity include abi1-1, abi2-1, ost1, gca2, and slac1 (Tian et al., 2015; Wang et al., 2016; Nilson & Assmann, 2007; Young et al., 2006). Arabidopsis mutants abi1-1 and abi-2 have been shown to have cooler leaves due to an inability to close stomata in response to drought (Merlot et al., 2002).

Ablation of gene function of OST1 and GHR1, kinases that phosphorylate key anion channels as part of the ABA-response also produce mutants with altered leaf temperatures (He et al., 2018; Hõrak et al., 2017; Matrasova et al., 2015; Munemasa et al., 2016). Mutations in ion channels SLAC1 and ALMT12, and mitogen-activated kinase 12 (MPK12) have also been shown to impair guard cell responses to ABA and CO_2 as well as control over leaf temperature (Jakobson et al., 2016; Chen et al. 2017; Chater et al., 2015).

Mutants that exhibit ABA-independent CO_2 insensitivity that have been characterized in Arabidopsis. Impaired function of BETA CARBONIC ANHYDRASE 1 and BETA CARBONIC ANYDRASE 4 (Wang et al., 2016; Engineer et al., 2016), MAP kinase MPK4 (He et al., 2018), and RHC1, a MATE-type malate transporter (He et al., 2018; Oosten et al., 2016), has been shown to lead to an inability to undergo high CO_2-induced stomatal closure, leading to cooler leaf temperatures after exposure to high CO_2. Mutants in HT1, a negative regulator of OST1 activation, has been shown to be CO_2-hyperrespoonsive, leading to elevated leaf temperatures (Matrosova et al., 2015; Hashimoto et al., 2006).

To date, there have not been any published mutants exhibiting CO_2-unresponsiveness and aberrant leaf cooling in *Brachypodium distachyon*. There is one barley mutant *cool* that was isolated using thermography due to its inability to undergo stomatal closure in response to exogenous ABA (Raskin and Ladyman, 1988), that has however not been molecularly characterized.

Grass stomata involve the recruitment of two lateral subsidiary cells that are thought to enhance stomatal response dynamics (Chen et al., 2017). Subsidiary cells are lined with a number of ion channels and are thought to act as ion sources, allowing for greater fluctuations in guard cell

turgidity and stomatal apertures. Raissig et al. (2017) identified the *sid* mutant that lacked subsidiary cells; *sid* in turn exhibited altered stomatal conductance due to reduced stomatal apertures. Arabidopsis has stomata that are patterned according to the one-cell spacing rule that is enforced by the EPIDERMAL PATTERNING FACTOR LIGAND (EPFL) family (Hughes et al., 2017). Unlike Arabidopsis, which organizes its stomata in a more scattered pattern, grass stomata are arranged in files; the signaling cascade responsible for grasses' patterning of cells into rows has yet to be revealed (Abrash et al., 2018). Grasses also encode EPFs in their genome. Hughes et al. (2017) showed that overexpression of the barley orthologue of EPF1 led to a decrease in stomatal density, similar to previously characterized Arabidopsis mutants, indicating conservation of stomatal developmental machinery components across species. Arabidopsis mutant in EPF ligand receptor TMM and subtilase enzyme SDD1 was shown to produce more stomata that clustered together, resulting in cooler temperatures (Yang & Sack, 1995; Vrablova et al., 2017). YODA is a MAPKKK and upstream regulator of stomatal fate establishment that has been identified in Arabidopsis and Brachypodium. Mutants in YODA display similar clustering of stomata phenotypes in both Arabidopsis and Brachypodium. Although stomatal densities were nearly twice that of wild type in Brachypodium, data for *yoda* leaf temperatures were not presented (Abrash et al., 2018). There have not been any published Brachypodium mutants with altered leaf temperatures compared to wild type. This may be due to improved responses of grass stomata and some compensatory mechanisms to optimize stomatal apertures that make it more difficult to detect changes in canopy leaf temperatures compared to controls (Rudall et al., 2017; Chen et al., 2017). More thermal imaging screens in Brachypodium targeting stomatal responses will be needed to fully elucidate grass stomatal dynamics and how these characteristics has allowed them to adapt to hotter, water scarce environments.

The 21 candidate lines that were isolated in this forward genetic screen were chemically mutagenized using ethyl methane sulfonate (EMS), which has been shown to produce a mutation approximately every 550 kb (Brkljacic et al., 2011; Till et al., 2003; Till et al., 2003; Dalmais et al., 2013), or a total of 500 mutations for a 272 Mb genome. These mutations are usually single base pair changes but may also be insertions or deletions (Comai and Henikoff, 2006). EMS mutagenized lines in effect may have a number of mechanisms that are impacted that may be involved in the phenotypes that led to the isolation of the 21 candidate lines.

Candidate lines that are sequenced to have mutations in common genes and that exhibit similar and specific stomatal conductance phenotypes may be allelic; crossing between these lines may be performed to determine whether the phenotype is observable in the F2 populations. For other lines, backcrossing to the parental background, BD21-3 and whole genome sequencing in a large quantity of bulked mutants with the phenotype in F2 plants (assuming the mutation is recessive) can be used for mapping of the causal mutation (recessive or dominant) in the F1 generation. CRSPR/CAS9 lines for candidate genes in Brachypodium can then be characterized to confirm whether the original phenotypes can be reproduced using targeted gene ablation of putative loci. Novel CO_2 sensing elements in Brachypodium can be analysed for gene synteny in wheat, barley, and rye and manipulated to fine-tune stomatal responses for crops in the field.

Thank you to Paulo Ceciliato for allowing presentation of his Licor gas exchange analyses for candidates 1, 10, and 15 in this Master's thesis manuscript. Also thank you to Felipe Rangel who helped conduct the forward genetic screen.

1.4 Methods

1.4.1 Growth conditions

Light intensity in the growth room was increased from 120 μE m^{-2} s^{-1} to 250 μE m^{-2} s^{-1} (O'Connor, 2017) for optimal Brachypodium growth following the forward genetic screen. Prior to finishing the screen, the soil was Professional Growing Mix. Following identification of the 21 candidates, the soil used to grow the plants was a mixture of vermiculite, perlite, and soil (1:1:2 respectively) for improved root growth (O'Connor, 2017). Plants were grown at 40% humidity, an average atmospheric CO_2 of 450 ppm and follow a 16h and 8h light and dark cycle, respectively. Prior to growth, seeds were cold treated for 1 week to encourage proper seed maturation.

1.4.2 Thermal Imaging at Ambient and High CO_2

A FLIR T650sc (FLIR Systems, Inc. Wilsonville, OR 97070 USA) series thermal imaging camera equipped with a 25° lens was used to capture images of 5 to 6-week-old healthy plants. The camera used an uncooled VoX microbolometer detector responsive to the short-wave infrared (7.5 – 13.0 μm). Specified temperature accuracy was 0.25°C at room temperature. Thermal imaging took place in the growth room where plants were grown for ambient CO_2 screens. High CO_2 thermal imaging took place after exposing plants to 900 ppm CO_2 for 3 hours in Conviron high CO_2 chambers.

1.4.3 Stomatal Development Analysis

The selection of the same leaf between plants at the same developmental stage and imaging of the same area of the leaf allows for comparison between different genotypes. In this protocol, we have chosen to select the 5th leaf of the longest stem and to image the center of the leaf within a 25 mm^2 area. A droplet of Loctite Professional Grade super glue was placed in the center of a 20x60 mm

coverslip. The abaxial side of the leaf was then placed oriented vertically on the coverslip making sure that the center of the leaf aligned with the glue droplet. Once allowed to dry for 10 minutes, the leaf was peeled away, leaving behind an epidermal layer of cells. Using another 20x60 mm coverslip, the epidermal peel was covered and the slides were turned upside down to image the back side of the abaxial layer using a Leica CTR5000 DIC microscope at 40x objective. two images were taken above and below the main vein of the leaf. Images were saved as TIFF files; stomatal indices were analyzed using ImageJ software (http://rsb.info.nih.gov/ij/). Statistical analyses were performed using one-way ANOVA test in Microsoft® Excel.

1.4.4 Licor Gas Exchange Analysis

Stomatal conductance (gs) was measured in leaves of 5- to 6-week-old plants using portable gas exchange systems (LI-6800, LI-COR, Lincoln, NE, USA), starting 2 h after growth chamber light onset. For intact single leaf ABA treatments, a LED light source set at 150 μmol m−2 s−1 (10% blue) and a chamber temperature of 21 °C was used. Leaves were equilibrated for 1 h at a relative humidity of 70–72%, airflow of 200 rpm and CO2 concentration of 400 ppm. After 1 hour, steady-state stomatal conductance was recorded 10 min before the addition of ABA to the petioles submerged in water at the indicated concentration. For stomatal conductance measurements of single intact leaf CO_2 responses, incoming relative air humidity was kept at 70% and the imposed changes in CO_2 concentration were applied as indicated. Leaves were attached to intact plants and were equilibrated for 2 h before the measurements. The data presented represent n≥3 leaves with each leaf from independent plants per genotype per treatment.

II. Investigating the Role of SBTs on Stomatal Development in *Brachypodium distachyon*

2.1 Introduction

Brachypodium distachyon is a grass reference for the grain and biofuel crops wheat, rice, barley, and rye (Vogel & Bragg, 2009; Brkljacic et al., 2011) with a diploid genome of 272 Mb (Wang et al., 2013). The BD21 accession Brachypodium genome assembly was released in 2010 (The International Brachypodium Initiative, 2010); the Bd21-3 assembly was released in 2016 and is available at the Joint Genome Institute (JGI) website (https://genome.jgi.doe.gov/portal). The JGI website offers numerous avenues for functional and comparative genomics studies including Phytomine, an orthologue database that references genomes from all species. Phytozome is a genome database that includes 82 full sequenced plant species and provides annotation data for sequenced, T-DNA (Bragg et al., 2012), EMS and Sodium-Azide (NaAz; NaZ) mutagenized lines for BD21-3. *Brachypodium distachyon* mutagenized with NaAz have on average 1 mutation per 400 kb (approximately 700 mutations total; Dalmais et al., 2013). Mutagenized populations are sequenced using TILLING (Targeted Induced Local Lesions in Genomes) which utilizes a specialized endonuclease that recognizes mismatches, facilitating identification of mutated PCR amplicons. The Phytozome platform has been used in several published reverse genetic studies (Wang et al. 2013; Comai & Henikoff, 2006).

Stomatal development has been well characterized in the reference plant *Arabidopsis thaliana*. Stomatal development involves the coordinated transition between cell fates in series with asymmetric and symmetric divisions (Chater et al., 2015; Dong et al., 2009; MacAllister et al., 2007; Abrash & Bergmann, 2010; Abrash et al., 2011; Bergmann, 2004). bHLh (basic-helix-loop-helix) transcription factors SPCH (Lau et al., 2014), SCRM(ICE1)/SCRM2 (Jo & Dong et al., 2013), MUTE (MacAllister et al., 2007), and FAMA (Matos et al., 2014) have been identified to be key regulators of cell identity establishment that can be inactivated by MAPK

phosphorylation (Bergmann et al., 2004; Peterson et al., 2010). Small signaling peptides belonging to the EPF (EPIDERMAL PATTERNING FACTOR) family both positively and negatively regulate stomatal development in leaves (Lee et al., 2015; Katsir et al., 2011). EPF2 acts earlier in the stomata lineage to discourage adjacent stem-cell-like meristemoid cells from differentiating into stomata, ensuring proper spacing (Han & Torii, 2016; Peterson et al., 2010). EPF1 is expressed in committed guard mother cells (GMC) to further enforce the one-cell-spacing rule between stomata (Hara et al., 2007; Qi et al., 2017; Váten & Bergmann, 2012; Rudall et al., 2017). STOMAGEN (EPFL9) and CHAL (EFPL6) have been observed to promote stomatal differentiation (Hunt et al., 2010; Abrash et al., 2010). The EPF signal is received and transduced by ERECTA (ER)-like leucine rich repeat (LRR) receptor-like kinases (RLKs) and the LRR-like receptor protein TMM (Ho et al., 2016; Peterson et al., 2010; Shimada et al., 2011), leading to activation of the MAPKKK YODA, MPKK 4/5, and MPK3/6 (Bergmann et al., 2004; Peterson et al., 2010; Wengier et al., 2018) signaling cascade that negatively regulates stomatal fate establishment. The subtilase STOMATAL DENSITY AND DISTRIBUTION1 (SDD1) was observed to negatively regulate stomatal density through its activity with TMM (Berger & Altmann, 2000; Vrablova et al., 2017); however, its substrate remains to be identified (Peterson et al., 2010). CO_2 has also been shown to be a powerful modulator of stomatal development (Casson et al., 2010; Doheny-Adams et al., 2012). Engineer et al. (2014) performed RNA seq transcriptomics and apoplast proteomics revealing that EPF2 transcripts are not present in BETA CARBONIC ANHYDRASE 1,4 Arabidopsis mutants while they are in wild type; apoplast proteomic studies revealed that the extracellular protease, SBT 5.2 (CRSP; CO_2 RESPONSE SECRETED PROTEASE) was expressed in plants exposed to high CO_2 and not in ambient CO_2 controls. Follow up in vitro studies determined that SBT 5.2 (CRSP) cleaved and activated EPF2

(Engineer et al., 2014). In Arabidopsis, the HIC gene was identified to limit stomatal density at high CO_2 (Gray et al., 2000); *hic* mutants displayed higher stomatal density when grown at CO_2 than the parental ecotype C24. HIC encodes an enzyme involved in synthesizing of fatty acid chains; it is unclear how this gene product factors into the CO_2 controlled stomatal development module but it is hypothesized to participate in communication between cells for proper stomatal distribution (Gray et al., 2000).

Orthologues of key stomatal developmental regulators in Arabidopsis have been identified in maize, barley, rice and Brachypodium. In maize, overexpression of SDD1 led to decreased stomatal density, analogous to mutants identified in Arabidopsis (Liu et al., 2015). Overexpression of EPF1 in barley also led to a decrease in stomatal numbers (Hughes et al., 2017). The bHLh rice orthologue OsFAMA was shown to act in the same capacity of terminal stomatal differentiation when expressed in Arabidopsis (Glover, 2000; Liu et al, 2009). In Brachypodium, the bHLh transcription factor orthologues BdSPCH, BdICE1/SCRM2 first identified in Arabidopsis were shown to have slightly divergent functions in coordinating stomatal fate establishment (Raissig et al, 2016; Raissig et al., 2017); however, they exhibit a similar global regulation of the cell fate establishment module as they are still subject to regulation by MAPK phosphorylation (Raissig et al., 2016). Abrash et al. (2018) showed that loss of function of the MAPKKK YODA in Brachypodium leads to clustering of stomata, consistent with *yoda* phenotypes observed in Arabidopsis. While MAPK regulation of stomatal identity is initiated in Arabidopsis through subtilase involvement in processing EPFs which in turn provide information on proximity for proper stomatal distribution (Abrash et al., 2018), the mechanism through which stomatal density and patterning is regulated in Brachypodium remains speculative. Further investigation of putative upstream regulators of stomatal fate establishment

in Brachypodium is needed. Here subtilase (SBT) genes in Brachypodium are being investigated for their role in regulating stomatal density.

2.2 Results

2.2.1 Arabidopsis SBT Orthologues and Proteomic/Transcriptomic Analyses in Brachypodium (Felix Hauser, Jingbo Zhang, Erin Schitke)

A list of the 56 annotated subtilase genes in *Arabidopsis thaliana* was obtained from the publication by Rautengarten et. al. 2005. Using the orthologue database available on the phytomine website (https://phytozome.jgi.doe.gov/phytomine/begin.do), orthologous subtilase genes in *Brachypodium distachyon* (20 loci) were found (Felix Hauser, unpublished).

In previous proteomic experiments in the Schroeder laboratory for Brachypodium, wheat and rice, several peptides derived from SBT proteases including SBT1.7, SBT1.8, SBT1.9, SBT1.3 and SBT5.2 were identified. SBT1.7 was the most abundant protease in wheat, Brachypodium, and rice (Jingbo Zhang, unpublished data). The subtilisin-like protease 1.7 (SBT1.7) contributes to seed coat mucilage development in Arabidopsis (Rautengarten et al., 2005). SBT1.7 is in the same sub-clade as SDD1 (SBT1.3), which has been shown to negatively regulate stomatal density in the Arabidopsis C24 accession (Berger & Altmann, 2000). RNA-seq data for *Brachypodium distachyon* BD21-3 showed that transcript levels for SBT gene family orthologues 5.3 and 1.7 (lower expression), 5.2, and 1.8 (highest expression) were elevated in 10 day old plants grown for five days under low (150 ppm) and high (900 ppm) CO_2 conditions (Erin Schitke, unpublished). Homology between genes in these families is shown in figure 2.1.

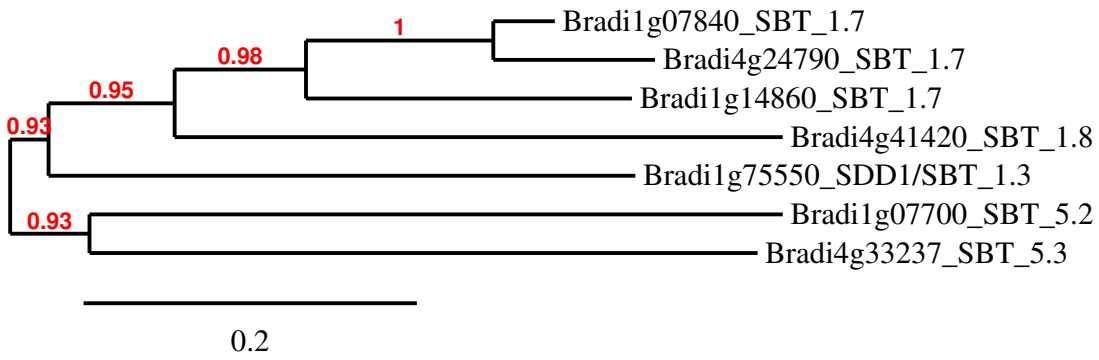

Figure 2.1: Phylogenetic tree of Transcript Sequences of genes in SBT families 1.3, 1.7, 1.8, 5.2, and 5.3

Transcript sequences for genes in SBT families 1.3, 1.7, 1.8, 5.2 and 5.3 were obtained from JGI Phytozome and input into a phylogenetic tree generator (Dereeper et al., 2008; Dereeper et al., 2010) to assess the homology amongst genes being investigated for their role in stomatal development in *Brachypodium distachyon*.

2.2.2 Genotyping of Brachypodium T-DNA insertion lines for genes in SBT families 1.3, 1.7, 1.8, 5.2, 5.3 was unsuccessful

Sequenced Brachypodium BD21-3 T1 T-DNA insertion lines for SBT5.2 (CRSP), SBT5.3 and SBT1.7 were obtained from John Vogel at the JGI institute, although genotyping of these T-DNA lines did not yield confirmation of a T-DNA insertion. After consulting a member of the Vogel lab, it was determined that this could have been due to the comparison of T-DNA lines with the parental background in BD21-3 to the accession genome BD21 to determine the location of the insert following sequencing, therefore accounting for mis-annotations of the presence of the T-DNA insert, or that the seeds that were sent did not contain the expected T-DNA insertion due to decreased transmission or lethality.

Genotyping was carried out according to a protocol from the John Vogel lab (Bragg et al. 2012). This involved using primers to amplify the Hygromycin resistance gene (HYG) purportedly present in the T-DNA construct in these lines. The reaction was performed in parallel to a positive control plasmid (pJJ2LBA) that was used to transform a large majority of the lines obtained (table 2.1). Gene specific primers sets were designed to bind 600-750 bp upstream and downstream of the predicted insert site to see if amplification of the gene region was abrogated. Gene-specific primer sets were used in combination with T3 LB and R9 RB T-DNA primers, accounting for different possible orientations of the insert within the genome, to see if a chimeric product could be obtained. In summary, 17 lines were genotyped to be wild type as the T-DNA insert could not be confirmed (figure 2.2).

Table 2.1: T1 T-DNA lines for SBT 1.3, 1.7, 1.8, 5.2 and 5.3

T1 T-DNA lines were ordered from JGI for genes in SBT families 1.3, 1.7, 1.8, 5.2, and 5.3 (column 2) based on Arabidopsis orthologues (columns 6, 7, 8). T-DNA lines (column 1) were transformed using either pJJ2LBA, pOL001, pJ22LB, or UbiBAR plasmid constructs (column 4) and sequenced by JGI Phytozome and determined to contain an insert (column 3) in exon, 3' UTR, intron, or intergenic regions.

T-DNA line	Gene Tagged	Insert Class	Construct	T-DNA orientation	best Arabidopsis TAIR10 hit name	best Arabidopsis TAIR10 hit symbol
JJ9855	Bradi1g07700	exon	pJJ2LBA	+	AT1G20160.1	ATSBT5.2
JJ16860	Bradi1g36242	exon	pJJ2LBA	-	AT2G04160.1	AIR3
JJ27518	Bradi2g10727.1	three_prime_UTR	pJJ2LBA	+	AT1G20160.1	ATSBT5.2
JJ11114	Bradi3g20580	near	pJJ2LBA	-	AT2G04160.1	AIR3
JJ13925	Bradi4g33237	intron	pJJ2LBA	-	AT2G04160.1	AIR3
JJ27951	Bradi1g07840.1	near	pJJ2LBA	-	AT5G67360.1	ARA12
JJ28173	Bradi1g07840.1	near	pJJ2LBA	-	AT5G67360.1	ARA12
JJ21827	Bradi1g14860	near	pJJ2LBA	.	AT5G67360.1	ARA12
JJ28052	Bradi4g24790.1/Bradi3g30750.1	intron	pJJ2LBA	+	AT5G67360.1	ARA12
JJ10414	Bradi1g77260	exon	PJJ2LBA	.	AT1G04110.1	SDD1
JJ8056	Bradi3g19300	exon	PJJ2LBA	.	AT1G04110.1	SDD1
JJ8680	Bradi1g01455	exon	pJJ2LBA	-	AT5G10770.1	
JJ27324	Bradi1g19070.1	exon	pJJ2LBA	-	AT3G54400.1	
CRC060	Bradi1g46190	near	pJJ2LBA	-	AT2G03200.1	
JJ19156	Bradi2g02120	exon	pJJ2LBA	+	AT1G03230.1	
JJ15, JJ1467, JJ135, JJ395, CRC288, CRC322, JJ1068	Bradi2g25850	exon	pOL001, pJJ2LB, UbiBAR, pOL001, pJJ2LBA, pJJ2LBA, pOL001	+	AT1G03220.1	
JJ14760, JJ15824, JJ24827, JJ16024, JJ16124, JJ16224, JJ16324, JJ16424, JJ16524, JJ16624	Bradi3g58850	exon	pJJ2LBA	-	AT2G03200.1	

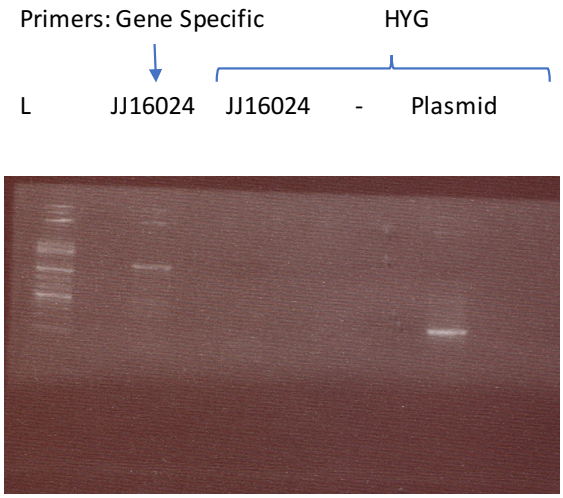

Figure 2.2: Example of genotyping results for *Brachypodium distachyon* T-DNA lines
PCR for T1 T-DNA lines for SBT 1.3, 1.7, 1.8, 5.2, and 5.3 showed consistent amplification of the gene using primers designed to bind approximately 600 base pairs upstream of the putative insertion site. Primers for the Hygromycin resistance gene present in the construct were used to determine the presence of the insert anywhere in the genome. A positive control plasmid for the Hygromycin gene was included to determine the efficacy of the primers. None of the T-DNA lines could be confirmed for a T-DNA insert.

2.2.3 TILLING: Using Sequence Indexed Sodium Azide lines from JGI Phytozome's Mutant Database to Investigate the role of SBTs 1.3, 1.7, 1.8, 5.2 and 5.3 in stomatal development in Brachypodium

Based on proteomic analyses in wheat, *Brachypodium distachyon* and rice and RNAseq analyses (Erin Schitke, unpublished data), SBT5.2 (CRSP), SBT5.3, SBT1.8, SBT 1.3/SDD1 and SBT1.7 were selected for further analyses of manipulation of stomatal density in the grass *Brachypodium distachyon*. Previous genotyping experiments reported that Brachypodium T-DNA lines were not reliable (figure 2.2). Sequence-indexed Sodium Azide (NaAz; NaZ) mutagenized lines were therefore selected as an exploratory tool of the impact of SBTs on stomatal development in Brachypodium. Seeds for over 20 sequenced NaAz mutagenized lines were received from the Institute Jean-Pierre which were predicted to be homozygous for single amino acid substitutions in exons, introns and 3' UTR modifiers. The NaZ lines (NaN) have predicted mutations in the SBT 1.3 (Bradi1g75550), SBT 5.2 (Bradi1g07700), SBT 1.7 (Bradi1g07840, Bradi1g14860, Bradi4g29790), SBT 1.8 (Bradi4g41420), and SBT 5.3 (Bradi4g33237) gene families.

Arabidopsis mutants in TMM and SDD1 were observed to have cooler leaf temperatures due to increased stomatal densities (Vrablova et al., 2017). All lines underwent thermal imaging experiments prior to characterization of stomatal morphology and patterning and were observed to have wild type leaf temperatures (data not shown).

2.2.3.1 Genotyping NaZ Lines for SBTs in Brachypodium

In November 2018, the JGI Phytozome database updated its mutant loci annotation reference (v3) for the BD21-3 v1 assembly to filter out sequenced lines that are not predicted to have impactful mutations (https://phytozome.jgi.doe.gov/pz/portal.html) using SnpEff Variant Annotation software (http://snpeff.sourceforge.net/SnpEff_manual.html). SnpEff define

impactful mutations in exon regions as those resulting in missense, nonsense amino acid changes or frameshifts. SnpEff analyses are not linked to protein structure databases so predictions of the impact of missense mutations on protein function are strictly putative. Lines that are not expected to have impactful mutations are annotated as "not impactful (v3)" in column 2 of tables 2.3 and column 4 of table 2.4.

Genotyping these NaAz lines has included DNA extraction, PCR using gene specific primers, and sending purified PCR products for Sanger sequencing. Results were obtained using a minimum of 3 high quality reads of the mutant locus regions (tables 2.2, 2.3, and 2.4). Previously, primers were designed using the NCBI database *Brachypodium distachyon* assembly (https://www.ncbi.nlm.nih.gov/nuccore/1334373560) for improved base pair loci specificity and overall efficiency. Primers were designed to bind 300 bp upstream and downstream of the mutated loci that is described by its base pair position in the *Brachypodium distachyon* BD21-3 v1 genomic assembly available at JGI Phytozome's JBrowse (https://phytozome.jgi.doe.gov/pz/portal.html#!info?alias=Org_Bdistachyon). Sequencing data was first compared to the base pair region used to design the primers to find any discrepancies. However, when sequencing data was compared to the genomic region for the genes of interest in JGI Phytozome's BD21-3 v1 assembly, the sequences did not correspond due to differences in reference base pair loci annotations. Primers were then designed using the JGI Phytozome BD21-3 v1 genome assembly for all of the genotypes, as this assembly was more reliable as the annotation is newer and improved. Genomic DNA sequences could be found under the gene information in JB Browse. Sequences were copied and edited to flank the mutated loci by at least 150 bp. These sequences were then input into primer design software Primer3Plus (http://www.bioinformatics.nl/cgi-bin/primer3plus/primer3plus.cgi).

Blind stomatal imaging and analyses experiments were pursued for lines predicted to have mutations impactful to gene function. Results for N=1,2, 3 (experimental repeats) are summarized in table 2.2.

2.2.4 Phenotyping Experiments for NaZ line for Bradi1g14860 (SBT 1.7) and Bradi4g33237 (*SBT 5.3)*

In Arabidopsis, SDD1 and SBT 5.2 (CRSP) have been shown to negatively regulate stomatal density (Engineer et al., 2014). Orthologues for SDD1 and SBT 5.2 have been identified in Brachypodium (Felix Hauser, unpublished data; table 2.1). SBT 1.7 and SBT 5.3 are in the same subclade as SDD1 and SBT 5.2, respectively, in Brachypodium (figure 2.1).

The NaZ line (NaN) 310 was confirmed to have amino acid changes in Bradi1g14850 and Bradi4g33237 (R19E and S247Y, respectively; table 2.2). Sequencing results for every line for Bradi1g14860 did not align with the predicted mutations published at the JGI Phytozome database (tables 2.2, 2.3, 2.4). Further genotyping experiments will be needed to troubleshoot non-alignments of sequencing results. Sequencing results for Bradi4g33237 did overlap with the predicted amino acid change for the NaN 310 line. SnpEff predicts missense to be impactful to gene function, however SnpEff analyses do not account for 3D protein structure so predictions of the impact of missense mutations on protein function are speculative.

Following genotyping, stomatal index/density was investigated for NaN 310 in two independent blind experiments. NaN 310 was grown alongside BD21-3 for five weeks. 28 days after germination (scored as cotyledon emergence), the 4th leaf was selected from individual plants from the NaN 310 and BD21-3 lines and imaged using DIC microcopy (40x objective). Stomata for NaN 310 displayed wild-type stomatal spacing and morphology (figure 2.3 A). Pavemental cell and stomatal numbers were quantified using ImageJ software. Nan 310 may have an increased number of stomata compared to wild type ($P<0.05$; figure 2.3 C).

A

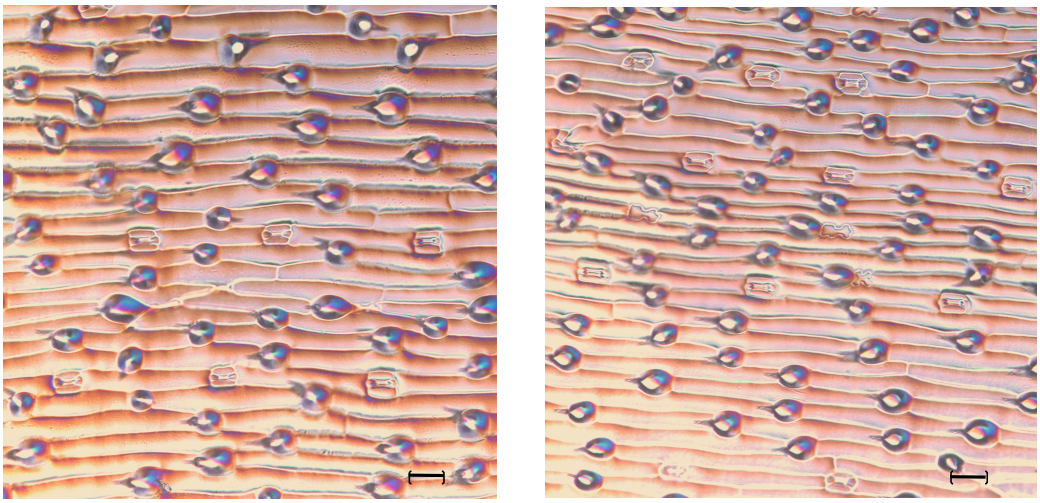

B

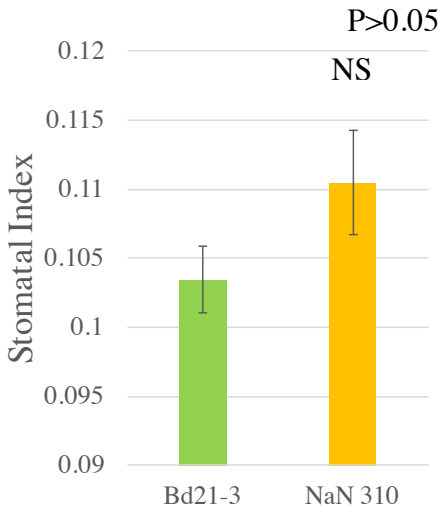

C

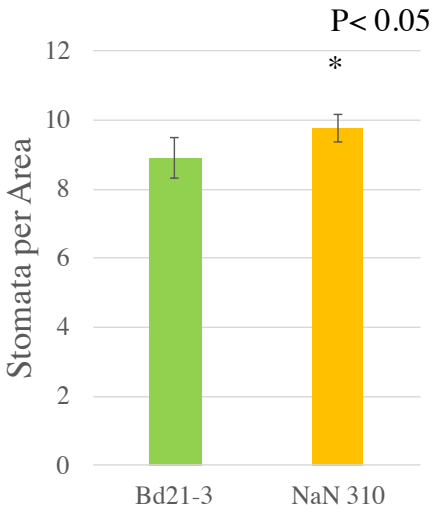

Figure 2.3: Stomatal imaging and index/density calculations for sodium azide (NaZ) mutagenized line NaN 310 for Bradi4g33237 (SBT 5.3) and Bradi1g14860 (SBT 1.7)

Stomatal spacing and morphology for NaN 310 is wild-type(A). Average B) stomatal index and **C)** stomatal density ± standard deviation was calculated using N=2 experimental repeats of a minimum of n≥5 plants per line, 4 images each plant, for the 4th true leaf from the NaN 310 and parental (BD21-3) lines 28 dag (days after germination). Leaves were imaged at 40x magnification; calibration bar corresponds to 20 μm. Associated p-value is B) 0.21 C) 0.047 for NaN 310 and BD21-3 (single factor ANOVA test (Tukey's)).

2.2.5 Selection of most promising lines for investigation of the role of SBTs in stomatal development in Brachypodium

Prior to the SnpEff variant annotation update to the BD21-3 v1 genome assembly, genotyping experiments were being pursued for all the NaZ lines that were ordered for SBT 1.7, 1.8, 1.3, 5.2, and 5.3 (table 2.3). Phenotyping experiments were not pursued for lines that could not be confirmed for a mutation in the predicted mutated loci.

One line (NaN 1688; table 2.2) was predicted to have a premature stop codon for Bradi1g75550 (SDD1/SBT 1.3); however, so far none of lines ordered for the gene could be confirmed for their sequenced (or any) mutation and genotyping experiments are still ongoing (table 2.3). The lines predicted to have impactful mutations are summarized in table 2.2. Following the genome annotation update, phenotyping experiments were only pursued for lines that could be confirmed for impactful mutations. Some of these lines (NaN 1949, NaN 418) could not be phenotyped due to low germination rates.

Table 2.2: Summary of most promising NaZ lines based on previous genotyping and preliminary phenotyping experiments, continued.

All lines presented in this table are expected to have impactful mutations based on sequencing data that is compared to JGI Phytozome's mutated loci impact analysis update released in November 2018.

**An "'x" in this column indicates that thermal imaging g experiments were performed for this line.

***Additional comments may be present in this column if issues with germination were encountered for a given line, impacting expedience of future experiments. An empty cell in these columns indicate that the genotype has low yield/germination rates and more seeds needed to be ordered.

NaN2062 Bd1:5689808..56898 10 (Hom)	**NaN310** Bd4:39154931..391549 33 (Hom)	**NaN310** Bd1:11974571..11 974573 (Hom)	**NaN87** Bd1:11976652 ..11976654 (Hom)	**NaN2011** **Position** Bd1:11974586.. 11974588 (Hom)	**NaN1688** Bd1:73037680 ..73037682 (Hom)	NaN Lines Loci
Bradi1g07840	Bradi4g33237	Bradi1g14860	Bradi1g14860	Bradi1g14860	Bradi1g75550	Gene of Interest
SBT 1.7	SBT 5.3	SBT 1.7	SBT 1.7	SBT 1.7	SDD1/SBT 1.3	Gene Family
synonymous gaG/gaA E193 gTg/gGg V254G Tgc/Ggc C255G	tCc/tAc S247Y	aAG/aGA R19E	unconfirmed	Gtc/Atc V102I	unconfirmed	Amino Acid/Codon Change
wild type-like	wild type-like		wild type-like	wild type-like	wild type-like	Thermal Imaging
N=3	N=2		N=2	N=2	N=1, low germination	DIC stomatal imaging e (preliminary, N=1, N=2, N=3***
wild-type	more stomata					Stomatal Development Phenotype

Table 2.2, cont'd

NaN Lines Loci	**NaN418** Bd4:39154234..39154236 (Hom)	**NaN448** Bd4:45694124..45694126 (Hom)	**NaN1794** Bd1:5573363..5573365 (Hom)	**NaN423** Bd1:5573327..55 73329 (Hom)	**NaN1949** Bd1:5573606..5 573608 (Hom)	**NaN397** Bd4:30100874..3 0100876 (Hom)
Gene of Interest	Bradi4g33237	Bradi4g41420	Bradi1g07700	Bradi1g07700	Bradi1g07700	Bradi4g24790
Gene Family	SBT 5.3	SBT 1.8	SBT 5.2	SBT 5.2	SBT 5.2	SBT 1.7
Amino Acid/Codon Change	Gtg/Ttg V112L	gCg/gTg A567V	Gag/Aag E277K	Gcg/Acg A265T	Gcc/Acc A359T	gGc/gAc G307S
Thermal Imaging	wild type-like	wild type-like	wild type-like	wild type-like	wild type-like	wild type-like
DIC stomatal imaging e (preliminary, N=1, N=2,	low germination	N=1, low germination	N=3	N=3	low germination	N=1, low germination
Stomatal Development Phenotype			wild type	wild type		

Table 2.3: Summary table of genotyping data for NaZ lines sequenced for homozygous mutations in SBT genes 1.3, 1.7, 5.2, 1.8 and 5.3, continued.

Table 2.3 includes genotyping data annotated using the JGI Phytozome Bd21-3 v1.1 genome assembly and mutated loci impact analysis v3 (Nov 2018); genotyping data for lines that were determined to have non-impactful mutations following the November 2018 annotation update is also included. Genotyping experiments were no longer pursued for lines with non-impactful mutations.

* An '*' in this column indicates that the mutation determined by Sanger sequencing differed from the JGI Phytozome BD21-3 v1 assembly annotation of the mutant loci summarized in Table 2.4.

Table 2.3: Genotyping Results

NaN Lines Loci	Gene of Interest	Gene Family	Sequenced genomic region	Improved Genotyping Predicted Mutation *	Amino Acid Sequence/ Codon Change
NaN121 **Position** Bd1:73037325..73037327 (Hom)	Bradi1g75550	SDD1/SBT 1.3		unconfirmed*	
NaN83 **Position** Bd1:73036776..73036778 (Hom)	Bradi1g75550	SDD1/SBT 1.3		unconfirmed*	
NaN1914 Bd1:73037105..73037107 (Hom)	Bradi1g75550	SDD1/SBT 1.3		unconfirmed*	
NaN1688 Bd1:73037680..73037682 (Hom)	Bradi1g75550	SDD1/SBT 1.3		unconfirmed*	
NaN2011 **Position** Bd1:11974586..11974588 (Hom)	Bradi1g14860	SBT 1.7	Bd1: 11974338-11975008 670 bp	G706A*	Gtc/Atc V102I
NaN285 **Position** Bd1:11975328..11975330 (Hom	Bradi1g14860 not impactful v3	SBT 1.7		unconfirmed*	
NaN2083 Bd1:11973986..11973988 (Hom)	Bradi1g14860 (3'UTR) not impactful v3	SBT 1.7		unconfirmed*	

Table 2.3 continued

NaN Lines Loci	Gene of Interest	Gene Family	Sequenced genomic region	Improved Genotyping Predicted Mutation *	Amino Acid Sequence/ Codon Change
NaN1793 Bd1:11973966..11973968 (Hom)	Bradi1g14860 (3'UTR) not impactful v3	SBT 1.7		unconfirmed*	
NaN87 Bd1:11976652..11976654 (Hom)	Bradi1g14860	SBT 1.7		unconfirmed*	
NaN278 Bd1:11975920..11975922 (Hom)	Bradi1g14860	SBT 1.7		unconfirmed*	
NaN310 Bd1:11974571..11974573 (Hom)	Bradi1g14860	SBT 1.7	Bd1: 11974288-11974973 685 bp	AG459-460GA*	aAG/aGA R19E
NaN310 Bd4:39154931..39154933 (Hom)	Bradi4g33237	SBT 5.3	Bd4: 39154665-39155404 739 bp	C1274A	tCc/tAc S247Y
NaN2062 Bd1:5689808..5689810 (Hom)	Bradi1g07840	SBT 1.7	Bd1: 5689694-5690320 626 bp	G579A* T761G* T763G*	synonymous gaG/gaA E193 gTg/gGg V254G Tgc/Ggc C255G
NaN518 Bd1:5690065..5690067 (Hom)	Bradi1g07840 not impactful v3	SBT 1.7	Bd1: 5689691-5690320 629 bp	C838T	synonymous D172 gaC/gaT
NaN288 Bd1:5689788..5689790 (Hom)	Bradi1g07840	SBT 1.7	Bd1: 5689691-5690308 617 bp	unconfirmed*	

Table 2.3 continued

NaN Lines Loci	Gene of Interest	Gene Family	Sequenced genomic region	Improved Genotyping Predicted Mutation *	Amino Acid Sequence/ Codon Change
NaN182 Bd4:30099795..30099797 (Hom)	Bradi4g24790 (3' UTR) not impactful v3	SBT 1.7	Bd4: 30099735-30100102 367 bp	C142T	
NaN397 Bd4:30100874..30100876 (Hom)	Bradi4g24790	SBT 1.7	Bd4: 30100782-30101393 611 bp	G1221A*	G307S gGc/gAc
NaN1949 Bd1:5573606..5573608 (Hom)	Bradi1g07700	SBT 5.2	Bd1: 5572818-5573651 833 bp	G1609A	A359T Gcc/Acc
NaN122 Bd1:5572364..5572366 (Hom)	Bradi1g07700 (intron) not impactful v3	SBT 5.2	Bd1: 5572199-5572778 579 bp	G366A	
NaN423 Bd1:5573327..5573329 (Hom)	Bradi1g07700	SBT 5.2	Bd1: 5572809-5573683 874 bp	G1329A	A265T Gcg/Acg
NaN1794 Bd1:5573363..5573365 (Hom)	Bradi1g07700	SBT 5.2	Bd1: 5572845-5573789 944 bp	G1366A	E277K Gag/Aag
NaN248 Bd1:5572973..5572975 (Hom)	Bradi1g07700 not impactful v3	SBT 5.2	Bd1: 5572848-5573788 940 bp	C976T	synonymous ggC/ggT G178
NaN448 Bd4:45694124..45694126 (Hom)	Bradi4g41420	SBT 1.8	Bd4: 45693940-45694590 654 bp	C3722T	gCg/gTg A567V
NaN418 Bd4:39154234..39154236 (Hom)	Bradi4g33237	SBT 5.3	Bd4: 39153993-39154427 434 bp	G991A* G1054A* G577T	synonymous synonymous Gtg/Ttg V112L

2.3 Discussion

Utilizing JGI Phytozome's sequence indexed mutant database, one line, NaN 310, with point mutations in exons for Bradig14860 (SBT 1.7) and Bradi4g33237 (SBT 5.3) resulting in amino acid changes was identified. Stomatal imaging experiments have begun to reveal that NaN 310 may have an increase in stomatal numbers. Dominant negative transgenic lines such as CRSPR/cas9 lines for Bradi1g14860 and Bradi4g33237 could help characterize the impact of these SBTs in stomata development.

As of yet, the role of subtilase enzymes in stomatal development in Brachypodium has not been characterized. *sdd1* mutants in Arabidopsis were observed to have increased stomatal densities (Vrablova et al., 2017), indicating SDD1 is a negative regulator of stomatal development. It remains unclear how SDD1 represses stomatal development as its substrate has not been identified. One proposed model involves proteolytic inactivation of a peptide promoter of entry into the stomatal lineage program STOMAGEN, by SDD1 (Hara et al., 2007; Schaller et al., 2012; Peterson et al., 2010), although further studies into SDD1's capacity to cleave STOMAGEN are needed. SBT 5.2 (CRSP) protease cleaves EPF2 in Arabidopsis to down-regulate stomatal development under elevated CO_2 conditions (Engineer et al., 2014).

Members of the EPF family of signaling peptides have been found to positively and negatively regulate stomatal differentiation (Rowe et al., 2010; Rychel et al., 2010; Bergmann, 2004; Peterson et al., 2010). So far, 4 EPFs have been identified to participate in stomatal development in the leaf epidermis. EPF1 and EPF2 act at different stages of the stomatal differentiation programs to inhibit clustering of stomata (Liu et al., 2015) while STOMAGEN (EPFL9) and CHAL (EPFL6) have been observed to act in the opposite capacity as overexpression lines lead to increased stomatal numbers (Hunt et al., 2010; Abrash & Bergmann,

2010); however, it is unclear what mechanism initiates the secretion and activation of EPF peptides.

Over 20 sequenced-indexed Sodium-Azide (NaZ) mutagenized lines for SBTs 1.3, 1.8, 1.7, 5.2, and 5.3 were ordered to investigate the role of SBTs in stomatal development in *Brachypodium distachyon*. Genotyping results for these lines were at times inconsistent with the predicted mutations published at the JGI Phytozome database and genotyping experiments are still ongoing. Nonetheless, 10 lines (table 2.2) that were sequenced and predicted to have missense mutations denoted impactful according to SnpEff Variant annotation software were selected for further phenotyping analyses of stomatal morphology and distributions. Stomatal imaging experiments consisted of a minimum of 3 plants per experimental repeat. Experimental repeats (N=x) were used for conducting analyses of stomatal patterning to ensure reproducibility of data. Stomatal development has been shown to be highly subject to environmental conditions such as light (Lau & Bergmann, 2012) in Arabidopsis, so growth conditions were kept uniform across experimental repeats. Furthermore, all plants undergoing stomatal assessments were made sure to be similar of stature and overall appearance. A minimum sample size of 3 plants per experimental repeat was used for phenotyping NaZ lines summarized in table 2.2. Some lines (NaN 1949, NaN 418) could not be phenotyped or could only undergo preliminary stomatal analyses (NaN 448, NaN 1688, NaN 397) due to low germination rates. N=3 and N=2 stomatal imaging experiments for NaN 423, 1794, NaN 2062, and Nan 2011, and NaN 87, respectively, showed normal stomatal numbers. N=2 stomatal imaging experiments for NaN 310 showed that this line may have an increased stomatal density compared to wild type. NaN 310 should be selected for more stomatal index and density analyses with an increased sample size to see if results can be reproduced. Although NaN 1688 line could not be confirmed for the predicted

premature stop –codon, follow-up genotyping experiments such as sequencing of the whole Bradi1g75550 gene may be beneficial as the occurrence of having a nonsense mutation in a gene of interest in a TILLING population is rare. It is for this reason that the line was selected to undergo preliminary stomatal imaging experiments. The inability to confirm predicted mutations may either be due improper primer design, false positives generated by the TILLING method for identifying mismatched base pairs or an inaccuracy in base pair calling in the reference genome.

Published mutants identified to have an increased stomatal index or density, such as the *Brachypodium distachyon* mutant *yoda* (Abrash et al., 2018), *Arabidopsis thaliana* mutants *sdd1* (Berger & Altmann, 2000), *er erl1 erl2* (Shapak et al., 2004), *tmm* (Yang & Sack, 1995), *epf1* (Hara et al., 2007) and Arabidopsis overexpression lines for EPFL6 (Abrash et al., 2011) display concomitant clustering of stomata. Grasses organize the epidermal cells in their leaves into rows; stomata are distributed in discreet files according to the one-cell spacing rule (Bergmann, 2018). The mechanism through which grasses organize epidermal cells into rows, and determine which rows will contain stomata has not been well studied (Chater et al., 2017). Although the NaN 310 line displayed no obvious clustering of stomata, stomatal density, but not stomatal index, appeared to be elevated compared to wild type. This may be due to an increased frequency of stomata-containing rows, or a decreased size of pavemental cells.

Stomatal density has been implicated in transpirational rates in plants (Miglietta et al., 2011; Chaerle et al., 2005; Masle et al., 2005; Nilson & Assmann, 2007; Doheny-Adams et al., 2012). Hughes et al. (2017) found that overexpression of EPF1 in barley, resulting in a decrease in stomatal density, led to decreased wilting in water-scarce conditions. Understanding the machinery underpinning stomatal development presents a worthwhile avenue for the improvement of crops through genetic manipulation of stomatal density.

2.4 Methods

2.4.1 Primer Design

The T-DNA lines ordered from JGI were in the parental background BD21-3, but JGI sequenced the lines and compared them to the BD21 v3 genome as it was more up-to-date. However, differences in the genome annotations between BD21-3 and BD21 may have led to the mis-confirmation of the presence of a T-DNA insert in these sequenced lines, explaining how no T-DNA insert could be detected using genotyping techniques. Gene specific primers were designed to bind approximately 600 bp upstream and downstream of the putative insert loci using the BD21 v3 genome assembly available the NCBI database ((https://www.ncbi.nlm.nih.gov/nuccore/1334373560).

Primers for the NaZ lines with the parental background BD21-3 were originally designed using the NCBI BD21 v3 genome assembly (https://www.ncbi.nlm.nih.gov/nuccore/1334373560). However, sequencing using these primers revealed that the amplified regions did not correspond to expected mutated loci sequenced and published at JGI Phytozome's BD21-3 v1 genome assembly. Primers were redesigned to bind at least 150 bp upstream and downstream, of the expected mutated loci using genomic sequences obtained from JGI Phytozome (https://phytozome.jgi.doe.gov/pz/portal.html#!info?alias=Org_Bdistachyon) using primer design software Primer3Plus (http://www.bioinformatics.nl/cgi-bin/primer3plus/primer3plus.cgi). Analysis of genotyping results such as determination of primer binding and sequenced regions were conducted by assessing the position of the amplicon relative to the base pair position of the start of the gene.

2.4.2 Genomic DNA Extraction, Genotyping, and Sanger Sequencing

Genomic DNA was extracted from leaves from healthy plants. The leaves were put in 1.5 ml micro centrifuge tubes that were then submerged in liquid nitrogen. Two metallic beads were placed inside the tube along with the leaves; the tube was then mounted into a grinder set for 25 cycles per second for 1 minute and 30 seconds. After being re-submerged in liquid nitrogen, 300 µl of extraction buffer Plant DNAzol. After being put in the shaker for 5 minutes, the tubes were placed inside the centrifuge for 10 min. at 12,000xg. The supernatant was then transferred to 300 µl of 100 % ethanol in different 1.5 ml tubes. The tubes were then inverted 6-8 times and left to sit for 5 minutes to allow the DNA to condense, then centrifuged for 4 minutes at 5,000 xg. The supernatant was then discarded. 300 µl of a 3:1 ethanol-Plant DNazol wash was added to the tubes which were inverted 6-8 times, left to sit at room temperature for 5 minutes, followed by centrifugation for 4 min. at 5,000 xg. The supernatant was discarded and 300 µl 75% ethanol was added to the tubes, followed by centrifugation for 4 minutes at 5,000 xg. The supernatant was decanted and remaining liquid was micropipetted out. Making sure not to allow the pellet to dry, the DNA was dissolved in 50 µl L 8mM NaOH and placed in a -40C freezer.

Primers in table 2.6 and 2.7 were used for genotyping of putative T-DNA lines listed in table 2.1. Gene-specific primers were used in combination with the T3 T-DNA LB and the R9 T-DNA RB primers depending on the annotated orientation of the insert (table 2.1). HYG primers were also used as a control to detect the presence of the T-DNA insert anywhere inside the genome. A positive control plasmid pJJ2LBA that was used to transform the majority of the T-DNA lines that were ordered was used to test the efficiency of the HYG primers.

Primers in table 2.5 were used to genotype NaZ lines. PCR products were purified using Exonuclease I and Shrimp Alkaline Phosphatase and sent for Sanger sequencing. 3 high quality

reads (Q>300) were used to determine the presence of a mutation in the predicted loci and compared to the sequenced mutation detected by SnpEff Variant software (table 2.4).

2.4.3 Growth conditions

All lines were grown with a light intensity of 200 μE m^{-2} s^{-1} and 250 μE m^{-2} s^{-1} (O'Connor, 2017) for optimal Brachypodium growth. The soil used to grow the plants was a mixture of vermiculite, perlite, and soil (1:1:2 respectively) for improved root growth (O'Connor, 2017). Plants were grown at 40% humidity, at atmospheric CO_2 and follow a 16h and 8h light and dark cycle, respectively. Prior to growth, seeds were cold treated for 1 week to encourage proper seed maturation.

2.4.4 Thermal Imaging

A FLIR T650sc (FLIR Systems, Inc. Wilsonville, OR 97070 USA) series thermal imaging camera equipped with a 25° lens was used to capture images of 4-5-week-old healthy plants. The camera used an uncooled VoX microbolometer detector responsive to the short-wave infrared (7.5 – 13.0 μm). Specified temperature accuracy was 0.25°C at room temperature.

2.4.5 Microscopy and Cell Counts

The selection of the same leaf between plants at the same developmental stage and imaging of the same area of the leaf allows for comparison between different genotypes. In this protocol, the 4th leaf of the longest stem was selected to image the center of the leaf within a 25 mm^2 area. The abaxial side of the leaf was placed vertically on a 20x60 mm coverslip containing a droplet of Loctite Professional Grade super glue and allowed to dry for 10 minutes. Once dry, the leaf was

peeled away, leaving behind an epidermal layer of cells. The slide was turned upside down and placed upon another 20x60 mm coverslip to image the back of the abaxial layer of cells using a Leica CTR5000 DIC microscope at 40x objective, two images were taken above and below the main vein of the leaf. Images were saved as TIFF files; stomatal indices were analyzed using ImageJ software (http://rsb.info.nih.gov/ij/). Statistical analyses were performed using one-way ANOVA test in Microsoft® Excel.

Table 2.4: Summary of SnpEff mutant locus annotations and v3 mutated loci impact analysis data found at JGI Phytozome for BD21-3 v1 assembly for sequenced sodium azide lines for SBTs 1.3, 1.7, 1,8. 5.2, and 5.3, continued

Table 2.4: Summary of SnpEff mutant locus annotations

NaAz Lines Loci	Gene of Interest	Gene Family	Mutation Class and Impact	Codon Change	Amino Acid Change
Site: **NaN121_Bd1_73037326_Hom** **Position** Bd1:73037325..73037327 (Hom)	Bradi1g75550	SDD1/SBT 1.3	MISSENSE MODERATE	Ccg/Tcg	P187S
Site: **NaN83_Bd1_73036777_Hom** **Position** Bd1:73036776..73036778 (Hom)	Bradi1g75550	SDD1/SBT 1.3	MISSENSE MODERATE	Gtg/Atg	V370M
Site: **NaN1914_Bd1_73037106_Hom** **Position** Bd1:73037105..73037107 (Hom)	Bradi1g75550	SDD1/SBT 1.3	MISSENSE MODERATE	gCc/gTc	A260V
Site: **NaN1688_Bd1_73037681_Hom** **Position** Bd1:73037680..73037682 (Hom)	Bradi1g75550	SDD1/SBT 1.3	NONSENSE HIGH	tgG/tgA	W68* stop gained
Site: **NaN2011_Bd1_11974587_Hom** **Position** Bd1:11974586..11974588 (Hom)	Bradi1g14860	SBT 1.7	MISSENSE MODERATE	Gac/Aac	D718N
Site: **NaN285_Bd1_11975329_Hom** **Position** Bd1:11975328..11975330 (Hom	Bradi1g14860 not impactful (v3)	SBT 1.7	SILENT LOW	aaG/aaA	K470

Table 2.4 continued

NaAz Lines Loci	Gene of Interest	Gene Family	Mutation Class and Impact	Codon Change	
Site: NaN2083_Bd1_11973987_Hom **Position** Bd1:11973986..11973988 (Hom)	Bradi1g14860 (3'UTR) not impactful (v3)	SBT 1.7	UTR_3_PRIME MODIFIER LOW	C430T	
Site: NaN1793_Bd1_11973967_Hom **Position** Bd1:11973966..11973968 (Hom)	Bradi1g14860 (3'UTR) not impactful (v3)	SBT 1.7	UTR_3_PRIME MODIFIER LOW	G450A	
Site: NaN87_Bd1_11976653_Hom **Position** Bd1:11976652..11976654 (Hom)	Bradi1g14860	SBT 1.7	MISSENSE MODERATE	gCg/gTg	A29V
Site: NaN278_Bd1_11975921_Hom **Position** Bd1:11975920..11975922 (Hom)	Bradi1g14860	SBT 1.7	MISSENSE MODERATE	gCc/gTc	A273V
Site: NaN310_Bd1_11974572_Hom **Position** Bd1:11974571..11974573 (Hom)	Bradi1g14860	SBT 1.7	MISSENSE MODERATE	Gag/Aag	E723K

Table 2.4 continued

NaAz Lines Loci	Gene of Interest	Gene Family	Mutation Class and Impact	Codon Change	Amino Acid Change
Site: **NaN310_Bd4_39154932_Hom** **Position** Bd4:39154931..39154933 (Hom)	Bradi4g33237	SBT 5.3	MISSENSE MISSENSE MODERATE	tCc/tAc tCc/tAc	S240Y S247Y
Site: **NaN2062_Bd1_5689809_Hom** **Position** Bd1:5689808..5689810 (Hom)	Bradi1g07840	SBT 1.7	MISSENSE MISSENSE MODERATE	Gcc/Acc gCc/gTc	A87T A80V
Site: **NaN518_Bd1_5690066_Hom** **Position** Bd1:5690065..5690067 (Hom)	Bradi1g07840 not impactful (v3)	SBT 1.7	SILENT LOW	gaC/gaT	D172
Site: **NaN288_Bd1_5689789_Hom** **Position** Bd1:5689788..5689790 (Hom)	Bradi1g07840	SBT 1.7	MISSENSE MODERATE	gCc/gTc	A80V
Site: **NaN182_Bd4_30099796_Hom** **Position** Bd4:30099795..30099797 (Hom)	Bradi4g24790 (3' UTR) not impactful (v3)	SBT 1.7	UTR_3_PRIME MODIFIER LOW	C214T	
Site: **NaN397_Bd4_30100875_Hom** **Position** Bd4:30100874..30100876 (Hom	Bradi4g24790	SBT 1.7	MISSENSE LOW	gGc/gAc	G289D

Table 2.4 continued

NaAz Lines Loci	Gene of Interest	Gene Family	Mutation Class and Impact	Codon Change	Amino Acid Change
Site: NaN1949_Bd1_5573607_Hom **Position** Bd1:5573606..5573608 (Hom)	Bradi1g07700	SBT 5.2	MISSENSE MODERATE	Gcc/Acc	A358T
Site: NaN122_Bd1_5572365_Hom **Position** Bd1:5572364..5572366 (Hom)	(intron) not impactful (v3)	SBT 5.2	INTRON MODIFIER LOW	G791A	
Site: NaN423_Bd1_5573328_Hom **Position** Bd1:5573327..5573329 (Hom)	Bradi1g07700	SBT 5.2	MISSENSE MODERATE	Gcg/Acg	A265T
Site: NaN1794_Bd1_5573364_Hom **Position** Bd1:5573363..5573365 (Hom)	Bradi1g07700	SBT 5.2	MISSENSE MODERATE	Gag/Aag	E277K
Site: NaN248_Bd1_5572974_Hom **Position** Bd1:5572973..5572975 (Hom)	Bradi1g07700 not impactful (v3)	SBT 5.2	SILENT LOW	ggC/ggT	G178
Site: NaN448_Bd4_45694125_Hom **Position** Bd4:45694124..45694126 (Hom)	Bradi4g41420	SBT 1.8	MISSENSE MODERATE	gCg/gTg	A567V
Site: NaN418_Bd4_39154235_Hom **Position** Bd4:39154234..39154236 (Hom)	Bradi4g33237	SBT 5.3	MISSENSE MODERATE	Gtg/Ttg	V112L

Table 2.5: Primers used for genotyping of NaZ lines, continued.

Table 2.5: Primers for NaZ Lines

NaZ Line	JGI Phytozome BD21-3 v1 Loci	Primer sequences	Melting Temp. °C	Expected Product Size
NaN121	Bd1:73037325..73037327 (Hom)	TCCTCCGTAGCTCCTTCCTC TCCTCCGTAGCTCCTTCCTC	60.1 °C	652 bp
NaN83	Bd1:73036776..73036778 (Hom)	GGGAAACTGCATTCGAAAAA AGAGGTGCGTCACGTAGTCC	60.1 °C	483 bp
NaN1914	Bd1:73037105..73037107 (Hom)	TCCTCCGTAGCTCCTTCCTC TCCTCCGTAGCTCCTTCCTC	60.1 °C	651 bp
NaN1688	Bd1:73037680..73037682 (Hom)	GGACTACGTGACGCACCTCT TCCAGTACCCATGTCACTGC	59.6 °C	441 bp
NaN2011	Bd1:11974586..11974588 (Hom)	ATGCTAATGAGGCTGCTGCT CGAGCCAGCACACCTTGTA	60.1 °C	670 bp
NaN285	Bd1:11975328..11975330 (Hom	CTTCAGCTCCGACATCCTG GGGTCGGACGCTACATAAGA	59.5 °C	565 bp
NaN2083	Bd1:11973986..11973988 (Hom)	GTGGCAAAGTCCCAAAGGTA GCTACAAGGACGTGCGCTTA	60.0 °C	308 bp
NaN1793	Bd1:11973966..11973968 (Hom)	GTGGCAAAGTCCCAAAGGTA GCTACAAGGACGTGCGCTTA	60.0 °C	286 bp
NaN87	Bd1:11976652..11976654 (Hom)	GACACTCCAGTCTCCGTTCC ATCCCTTTCCATCATCACCA	53.7 °C	600 bp

Table 2.5 continued

NaN278	Bd1:11975920..11975922 (Hom)	AGAAGGTGTCCGGCAAGAT CGCAGAGGAAGTCCACGTA	59.7 °C	650 bp
NaN310	Bd1:11974571..11974573 (Hom) Bd4:39154931..39154933 (Hom)	ATGCTAATGAGGCTGCTGCT CGAGCCAGCACACCTTGTA CAGGTTTGCATCAGGCTACA GATGGACGGGTAGTTGAGGT	60.1 °C 58.9 °C	685 bp 739 bp
NaN2062	Bd1:5689808..5689810 (Hom)	GAGGACGTACATCGTCCACA CCCAGCACACCTTGTAGGTT	59.6 °C	626 bp
NaN518	Bd1:5690065..5690067 (Hom)	GAGGACGTACATCGTCCACA CCCAGCACACCTTGTAGGTT	59.6 °C	629 bp
NaN288	Bd1:5689788..5689790 (Hom)	GAGGACGTACATCGTCCACA CCCAGCACACCTTGTAGGTT	59.6 °C	617 bp
NaN182	Bd4:30099795..30099797 (Hom)	AGCTACTCCTCCCCACACAT GCGTGTCGTAGGTGTAGAGC	58.6 °C	367 bp
NaN397	Bd4:30100874..30100876 (Hom	TGTCCCTCTCACTTGGCGGC CCGGGCGTCACGGTTTTTGG	60.1 °C	611 bp
NaN1949	Bd1:5573606..5573608 (Hom)	AGCTCCACACAACCAGATCC CGACACGAACGATCAGAAAA	59.8 °C	833 bp
NaN122	Bd1:5572364..5572366 (Hom)	ATCTGCTTCGTCGTCGTTG GGAAATCCCAGGATCTGGTT	60.0 °C	579 bp
NaN423	Bd1:5573327..5573329 (Hom)	AGCTCCACACAACCAGATCC CGACACGAACGATCAGAAAA	59.8 °C	874 bp

Table 2.5 continued

NaN1794	Bd1:5573363..5573365 (Hom)	AGCTCCACACAACCAGATCC CGACACGAACGATCAGAAAA	59.8 °C	944 bp
NaN248	Bd1:5572973..5572975 (Hom)	AGCTCCACACAACCAGATCC CGACACGAACGATCAGAAAA	59.8 °C	940 bp
NaN448	Bd4:45694124..45694126 (Hom)	CAGTTCCTCGGTGCAACTTT TTTGCCCCAACTTCTTGAAC	54 °C	800 bp
NaN418	Bd4:39154234..39154236 (Hom)	TACATTGAAGCAACCACGTAAGA GCACTCTCGCTGCAAGAAA	59.7 °C	434 bp

Table 2.6: Gene-specific primers used for T-DNA lines, continued

Table 2.6				
T-DNA Line	Insertion Site BD21 v3 Genome Assembly	Gene Specific Primer Sequences	Melting Temp. °C	Expected Product Size
JJ27518	Bd2:8959824	CTGACGTACGTTCTGCCTGA CCATCCCATCTCTCTTTCCA	60.0 °C	1250 bp
JJ11114	Bd3:19629327	TGCCGTACAACCCTTACCTC GGGGATGCTCACACTAAGGA	60.1 °C	1619
JJ13925	Bd4:38885171	GACAACGGAGAGACACAGCA TTCGCAAGAATGTCAAGCAC	60.0 °C	1283 bp
JJ14760, JJ15824, JJ24827, JJ16024, JJ16124, JJ16224, JJ16324, JJ16424, JJ16524, JJ16624	Bd3:57951255	CTTTTGTGCGTCCCCTGTAT TTTTCTTGCCTGACCTGCTT	60.0 °C	1173 bp
JJ15, JJ1467, JJ135, JJ395, CRC288, CRC322, JJ1068	Bd2:24045495	GAAAGATGATGGCCGAGTGT GCCCTTACGCTGCAATAGAG	60.1 °C	1079 bp
JJ19156	Bd2:1452964	TGCTTGGTCAACCACATCAT CTCCTCATCGAGCACAACAA	60.0 °C	1381 bp
CRC060	Bd1:44657360	AAAGGATGGGAACTCGTGTG AGCACATGTGTGTCGTGGAT	60.0 °C	1190 bp
JJ28173	Bd1:5553087	CTTTTCCACGAATGGATGCT AAAATAATGGCACCGCTACG	60.1 °C	1190 bp
JJ21827	Bd1:11818823	GAGGGAGCACAAGAATGAGC GATTGCAGCTCTCCAAGGAC	60.0 °C	1018 bp
JJ28052	Bd4:29889567	GTTTGACCCGTTCGAGATGT GAGGTGCAGTGCTTTGTGAA	60.0 °C	979 bp
JJ10414	Bd1:73878341	TGCTGGTCTCAAACTCATCG GAGCAAACAATTCGGGAAAA	60.1 °C	1032 bp

Table 2.6 continued

JJ27324	Bd1:15278675	GCGTCGTCTTCATCTTCTCC TTACATTCATTCCCGCTTCC	60.0 °C	908 bp
JJ8056	Bd3:18044607	CAAGCGCTCACTAATGGACA CTGGCTACACCAATGGACCT	60.0 °C	1409 bp
JJ8680	Bd1:955543	TCCATGTGGTCAAAGCAGAG CCAGGCCCATCAAAGAATTA	59.9 °C	1064 bp
JJ9855	Bd1:5433063	GTACTACGGCCTGGCTTCAG GATCGGCGCATTAGTTGATT	60.1 °C	1290 bp
JJ16860	Bd1:32027665	ATTTTGATGGGCTCAGGTTG GGACGAGTTTTTGGCTTCAG	59.9 °C	1419 bp
JJ27951	Bd1:5552847	TTAGCGAAAGGCGAGTGAAT AAAATAATGGCACCGCTACG	60.0 °C	1419 bp

Table 2.7: T-DNA insert-specific primers

Hyg Fwd	ATGAAAAAGCCTGAACTCACCGCGAC
Hyg Rev	CTATTTCTTTGCCCTCGGACGAGTGC
T3 T-DNA LB	AGCTGTTTCCTGTGTGAAATTG
R9 T-DNA LB	GATAAGCTGTCAAACATGAGAATTCAG

References

Abrash, E. B., & Bergmann, D. C. (2010). Regional specification of stomatal production by the putative ligand CHALLAH. *Development*, *137*(3), 447 LP-455. http://dev.biologists.org/content/137/3/447

Abrash, E. B., Davies, K. A., & Bergmann, D. C. (2011). Generation of Signaling Specificity in Arabidopsis by Spatially Restricted Buffering of Ligand–Receptor Interactions. *The Plant Cell*, *23*(8), 2864 LP-2879. http://www.plantcell.org/content/23/8/2864.abstract

Abrash, E., Gil, M. X. A., Matos, J. L., & Bergmann, D. C. (2018). Conservation and divergence of YODA MAPKKK function in regulation of grass epidermal patterning, *Development*, *6*, 1–9. https://doi.org/10.1242/dev.165860

Assmann, S. M., & Jegla, T. (2016). Guard cell sensory systems: recent insights on stomatal responses to light, abscisic acid, and CO2. *Current Opinion in Plant Biology*, *33*, 157–167. https://doi.org/10.1016/j.pbi.2016.07.003

Benavente, E., Carrillo, J. M., & Quemada, M. (2013). Thermographic imaging: assessment of drought and heat tolerance in Spanish germplasm of Brachypodium distachyon. *Procedia Environmental Sciences*, *19*, 262–266. https://doi.org/10.1016/j.proenv.2013.06.030

Berger, D., & Altmann, T. (2000). A subtilisin-like serine protease involved in the regulation of stomatal density and distribution in Arabidopsis thaliana. *Genes and Development* 14:1119–1131.

Bergmann, D. C. (2004). Integrating signals in stomatal development,*Current Opinion in Plant Biology,* 7:26–32. https://doi.org/10.1016/j.pbi.2003.10.001

Bergmann, D. C. (2018). Quick guide Grass stomata. *Current Biology*, *28*(15), R814–R816. https://doi.org/10.1016/j.cub.2018.05.074

Bergmann, D. C., Lukowitz, W., & Somerville, C. R. (2004). Stomatal Development and Pattern Controlled by a MAPKK Kinase. *SCIENCE*, *304*(June), 1494–1498.

Bragg, J. N., Wu, J., Gordon, S. P., Guttman, M. E., Thilmony, R., Lazo, G. R., Gu, Y. Q., Vogel, J. P. (2012). Generation and Characterization of the Western Insertional Mutant Collection, *7*(9). https://doi.org/10.1371/journal.pone.0041916

Brkljacic, J., Grotewold, E., Scholl, R., Mockler, T., Garvin, D. F., Vain, P., Brutnell, T., Sibout, R.,Bevan, M., Budak, H., Caicedo, A. L., Gao, C., Gu, Y., Hazen, S. P., Holt III , B. F., Hong, S., Jordan, M., Manzaneda, A. J., Mitchell-olds, T., Mochida, K., Mur, L. A. J., Park, C., Sedbrook, J., Watt, M., Zheng, S. Jian., Vogel, J. P. (2011). Brachypodium as a Model for the Grasses: Today and the Future, *Plant Physiology*, *157*(September), 3–13. https://doi.org/10.1104/pp.111.179531

Casson, S. A., & Hetherington, A. M. (2010). Environmental regulation of stomatal development. *Current Opinion in Plant Biology*, *13*(1), 90–95. https://doi.org/https://doi.org/10.1016/j.pbi.2009.08.005

Chaerle, L., Saibo, N., & Straeten, D. Van Der. (2005). Tuning the pores: towards engineering plants for improved water use efficiency, *TRENDS in Biotechnology 23*(6). https://doi.org/10.1016/j.tibtech.2005.04.005

Chater, C. C. C., Caine, R. S., Fleming, A. J., & Gray, J. E. (2017). Origins and Evolution of Stomatal Development, *Plant Physiology*. *174*(June 2017), 624–638. https://doi.org/10.1104/pp.17.00183

Chater, C., Peng, K., Hedrich, R., Julie, E., Hetherington, A. M., Peng, Kai, Movahedi, M., Dunn, J. A., Walker, H. J., Liang, Y., Mclachlan, D. H., Casson, S., Isner, J. C., Wilson, I., Neill, S. J.(2015). Elevated CO 2 -Induced Responses in Stomata Require ABA and ABA Signaling. *Current Biology*, *25*(20), 2709–2716. https://doi.org/10.1016/j.cub.2015.09.013

Chen, Z.-H., Chen, G., Dai, F., Wang, Y., Hills, A., Ruan, Y.-L, Zhang, G., Franks, P. J., Nevo, E., Blatt, M. R. (2017). Molecular Evolution of Grass Stomata. *Trends in Plant Science*, *22*(2), 124–139. https://doi.org/10.1016/j.tplants.2016.09.005

Comai, L. & Henikoff, S. (2006). TILLING: practical single-nucleotide mutation discovery. *The Plant Journal*, (45), 684–694. https://doi.org/10.1111/j.1365-313X.2006.02670.x

Cotthem, V. A. N. (1970). A classification of stomatal types. *Bot. J. Linn. Soc.,* (63), 235–246. https://academic.oup.com/botlinnean/article-abstract/63/3/235/2725771

Dalmais, M., Antelme, S., Ho-Yue-Kuang, S., Wang, Y., Darracq, O., d'Yvoire, M. B., Cézard, L., Légée, F., Blondet, E., Oria, N., Troadec, C., Brunaud, V., Jouanin, L., Höfte, H., Bendahmane, A., Lapierre, C., Sibout, R. (2013). A TILLING Platform for Functional Genomics in Brachypodium distachyon. *PLOS ONE*, *8*(6), e65503. https://doi.org/10.1371/journal.pone.0065503

Dereeper A., Audic S., Claverie J.M., Blanc G. (2010). BLAST-EXPLORER helps you building datasets for phylogenetic analysis. *BMC Evol Biol*. Jan 12; 10:8.

Dereeper A.& Guignon V., Blanc G., Audic S., Buffet S., Chevenet F., Dufayard J.F., Guindon S., Lefort V., Lescot M., Claverie J.M., Gascuel O. (2008). Phylogeny.fr: robust phylogenetic analysis for the non-specialist. *Nucleic Acids Res*. Jul 1;36

Doheny-Adams, T., Hunt, L., Franks, P. J., Beerling, D. J., & Gray, J. E. (2012). Genetic manipulation of stomatal density influences stomatal size, plant growth and tolerance to restricted water supply across a growth carbon dioxide gradient, *Phil. Trans. R. Soc. B,* 547–555. https://doi.org/10.1098/rstb.2011.0272

Dong, J., Macalister, C. A., & Bergmann, D. C. (2009). BASL Controls Asymmetric Cell Division in Arabidopsis. *Cell*, *137*(7), 1320–1330. https://doi.org/10.1016/j.cell.2009.04.018

Engineer, C. B., Ghassemian, M., Anderson, J. C., Peck, S. C., Hu, H., & Schroeder, J. I. (2014). Carbonic anhydrases, EPF2 and a novel protease mediate CO2 control of stomatal development. *Nature*, *513*, 246. Retrieved from http://dx.doi.org/10.1038/nature13452

Engineer, C. B., Hashimoto-Sugimoto, M., Negi, J., Israelsson-Nordström, M., Azoulay-Shemer, T., Rappel, W.-J., Schroeder, J. I. (2016). CO2 Sensing and CO2 Regulation of Stomatal Conductance: Advances and Open Questions. *Trends in Plant Science*, *21*(1), 16–30. https://doi.org/10.1016/J.TPLANTS.2015.08.014

Girin, T., David, L. C., Chardin, C., Sibout, R., Krapp, A., Ferrario-méry, S., & Daniel-vedele, F. (2018). Brachypodium: a promising hub between model species and cereals. *Journal of Experimental Botany*, *65*(19), 5683–5696. https://doi.org/10.1093/jxb/eru376

Glover, B. J. (2000). Differentiation in plant epidermal cells. *Journal of Experimental Botany*, *51*(344), 497–505.

Gray, J. E., Holroyd, G. H., Lee, F. M. Van Der, Bahrami, A. R., Sijmons, P. C., Woodward, F. I., Schuch, W., Hetherington, A. M. (2000). The HIC signalling pathway links CO 2 perception to stomatal development. *Nature, 408*(December), 1998–2001.

Han, S., & Torii, K. U. (2016). Lineage-specific stem cells, signals and asymmetries during stomatal development, *Development, 1259*–1270. https://doi.org/10.1242/dev.127712

Hara, K., Kajita, R., Torii, K. U., Bergmann, D. C., & Kakimoto, T. (2007). The secretory peptide gene EPF1 enforces the stomatal one-cell-spacing rule, *Genes & Development*, 21: 1720–1725. https://doi.org/10.1101/gad.1550707.metric

Hashimoto, M., Negi, J., Young, J., Israelsson, M., Schroeder, J. I., & Iba, K. (2006). Arabidopsis HT1 kinase controls stomatal movements in response to CO2. *Nature Cell Biology*, *8*, 391. http://dx.doi.org/10.1038/ncb1387

He, J., Zhang, R., Peng, K., Tagliavia, C., Li, S., Xue, S., Liu, A., Hu, H., Zhang, J., Hubbard, K. E., Held, K., McAinsh, M. R., Gray, J. E., Kudla, J., Schroeder, J. I., Liang, Y., Hetherington, Alistair M Hetherington, A. M. (2018). The BIG protein distinguishes the process of CO (2) -induced stomatal closure from the inhibition of stomatal opening by CO (2) . *The New Phytologist*, *218*(1), 232–241. https://doi.org/10.1111/nph.14957

Hetherington, A. M., & Woodward, F. I. (2003). The role of stomata in sensing and driving environmental change. *Nature*, *424*(August), 901–908.

Ho, C. K., Paciorek, T., Abrash, E., Bergmann, D. C., Ho, C. K., Paciorek, T., Bergmann, D. C. (2016). Article Modulators of Stomatal Lineage Signal Transduction Alter Membrane

Contact Sites and Reveal Specialization among ERECTA Kinases. *Developmental Cell*, *38*(4), 345–357. https://doi.org/10.1016/j.devcel.2016.07.016

Hõrak, H., Sierla, M., Tõldsepp, K., Wang, C., Wang, Y., Nuhkat, M., Valk, E., Pechter, P., Merilo, E., Salojärvi, J., Overmyer, K., Loog, M., Brosché, M., Schroeder, J. I. (2016). A Dominant Mutation in the HT1 Kinase Uncovers Roles of MAP Kinases and GHR1 in CO 2 -Induced Stomatal Closure. *The Plant Cell*, *28*(October), 2493–2509. https://doi.org/10.1105/tpc.16.00131

Hu, H., Boisson-Dernier, A., Israelsson-Nordström, M., Böhmer, M., Xue, S., Ries, A.,Godoski, J., Kuhn, J. M., Schroeder, J. I. (2009). Carbonic anhydrases are upstream regulators of CO2-controlled stomatal movements in guard cells. *Nature Cell Biology*, *12*, 87. https://doi.org/10.1038/ncb2009

Hubbard, K. E., Siegel, R. S., Valerio, G., Brandt, B., & Schroeder, J. I. (2012). Abscisic acid and CO 2 signalling via calcium sensitivity priming in guard cells , new CDPK mutant phenotypes and a method for improved resolution of stomatal stimulus – response analyses. *Annals of Botany*, 5–17. https://doi.org/10.1093/aob/mcr252

Hughes, J., Hepworth, C., Dutton, C., Dunn, J. A., Hunt, L., Stephens, J, Waugh, R., Cameron, D. D., Gray, J. E. (2017). Reducing Stomatal Density in Barley Improves Drought Tolerance without Impacting on Yield, *Plant Physiology*, 174, (June), 776–787. https://doi.org/10.1104/pp.16.01844

Hunt, L., Bailey, K. J., & Gray, J. E. (2010). The signalling peptide EPFL9 is a positive regulator of stomatal development, *New Phytologist*, 186: 609–614 doi: 10.1111/j.1469-8137.2010.03200.x

Jakobson, L., Vaahtera, L., Kadri, T., Nuhkat, M., Wang, C., Wang, S., Hanna, H., Valk, E., Pechter, P., Sindarovska, Y., Tang, J., Xiao, C., Xu, Y., Talas, U. G., Garcı, A. T., Maran, U., Remm, M., Roelfsema, M R. G., Hu, H., Loog, M., Schroeder, J. I., Kollist, H. (2016). Natural Variation in Arabidopsis Cvi-0 Accession Reveals an Important Role of MPK12 in Guard Cell CO 2 Signaling, 1–25. https://doi.org/10.1371/journal.pbio.2000322

Jenks M. A,. Tuttle H. A, Eigenbrode S. D., Feldmann K. A. (1995). Leaf epicuticular waxes from the eceriferum mutants in Arabidopsis. *Plant Physiology* 108, 369±377.

Jo, L., & Dong, J. (2013). Stomatal Development in Arabidopsis. *The Arabidopiss Book*, 1–26. https://doi.org/10.1199/tab.0162

Katsir, L., Davies, K. A., Bergmann, D. C., & Laux, T. (2011). Peptide Signaling in Plant Development. *Current Biology*, *21*(9), R356–R364. https://doi.org/https://doi.org/10.1016/j.cub.2011.03.012

Keeling CD, Piper SC, Whorf TP, Keeling RF (2011) Evolution of natural and anthropogenic fluxes of atmospheric CO_2 from 1957 to 2003. Tellus B Chem Phys Meterol 63: 1–22

Kim, T., Maik, B., Hu, H., Nishimura, N., & Schroeder, J. I. (2010). Guard Cell Signal Transduction Network: Advances in Understanding Abscisic Acid , CO 2 , and Ca 2 + Signaling. *Annu. Rev. Plant Bio* 61:561–91. https://doi.org/10.1146/annurev-arplant-042809-112226

Lau, O. S., & Bergmann, D. C. (2012). Stomatal development: a plant ' s perspective on cell polarity , cell fate transitions and intercellular communication. *Development,* 3692, 3683–3692. https://doi.org/10.1242/dev.080523

Lau, O. S., Davies, K. A., Chang, J., Adrian, J., Rowe, M. H., Ballenger, C. E., & Bergmann, D. C. (2014). Direct roles of SPEECHLESS in the specification of stomatal self-renewing cells. *Science*, 345(6204), 1605–1610.

Lee, J. S., Hnilova, M., Maes, M., Lin, Y.-C. L., Putarjunan, A., Han, S.-K., Avila, J., Torii, K. U. (2015). Competitive binding of antagonistic peptides fine-tunes stomatal patterning. *Nature*, *522*, 439. https://doi.org/10.1038/nature14561

Leinonen, I., & Jones, H. G. (2004). Combining thermal and visible imagery for estimating canopy temperature and identifying plant stress. *Journal of Experimental Botany*, *55*(401), 1423–1431. Retrieved from http://dx.doi.org/10.1093/jxb/erh146

Liu, T., Ohashi-ito, K., & Bergmann, D. C. (2009). Orthologs of Arabidopsis thaliana stomatal bHLH genes and regulation of stomatal development in grasses. *Development*, 2276, 2265–2276. https://doi.org/10.1242/dev.032938

Liu, Y., Qin, L., Han, L., Xiang, Y., & Zhao, D. (2015). Overexpression of maize SDD1 (ZmSDD1) improves drought resistance in Zea mays L. by reducing stomatal density. *Plant Cell, Tissue and Organ Culture (PCTOC)*, *122*(1), 147–159. https://doi.org/10.1007/s11240-015-0757-8

MacAllister, C. A., & Bergmann, D. C. (2011). Sequence and function of basic helix--loop--helix proteins required for stomatal development in Arabidopsis are deeply conserved in land plants. *Evolution & Development, 192*, 182–192. https://doi.org/10.1111/j.1525-142X.2011.00468.x

MacAllister, C. A., Ohashi-ito, K., & Bergmann, D. C. (2007). Transcription factor control of asymmetric cell divisions that establish the stomatal lineage. *Nature* 445(February), 537–540. https://doi.org/10.1038/nature05491

MacAllister, C. A., & Bergmann, D. C. (2011). Sequence and function of basic helix--loop--helix proteins required for stomatal development in Arabidopsis are deeply conserved in land plants, *192*, 182–192. https://doi.org/10.1111/j.1525-142X.2011.00468.x

Masle, J., Gilmore, S. R., & Farquhar, G. D. (2005). The ERECTA gene regulates plant transpiration efficiency in Arabidopsis, *Nature*, Vol 436. https://doi.org/10.1038/nature03835

Matos, J. L., Lau, O. S., Hachez, C., Cruz-ramírez, A., Scheres, B., & Bergmann, D. C. (2014). Irreversible fate commitment in the Arabidopsis stomatal lineage requires a FAMA and RETINOBLASTOMA-RELATED module. *eLife*, 1–15. https://doi.org/10.7554/eLife.03271

Matrosova, A., Bogireddi, H., Mateo-Peñas, A., Hashimoto-Sugimoto, M., Iba, K., Schroeder, J. I., & Israelsson-Nordström, M. (2015). The HT1 protein kinase is essential for red light-induced stomatal opening and genetically interacts with OST1 in red light and CO2-induced stomatal movement responses. *New Phytologist*, *208*(4), 1126–1137. https://doi.org/10.1111/nph.13566

Merlot, S., Mustilli, A., Genty, B., North, H., Lefebvre, V., Sotta, B., Vavasseur, A., Giraudat, J. (2002). Use of infrared thermal imaging to isolate Arabidopsis mutants defective in stomatal regulation. *The Plant Journal*, *30*(5), 601–609. https://doi.org/10.1046/j.1365-313X.2002.01322.x

Miglietta F., Peressotti A., Viola R. , Korner C., and J. S. A. (2011). Stomatal numbers , leaf and canopy conductance , and the control of transpiration. *PNAS*, *108*(28), 2011. https://doi.org/10.1073/pnas.1105831108

Munemasa, S., Hauser, F., Park, J., Waadt, R., Brandt, B., & Schroeder, J. I. (2016). Mechanisms of abscisic acid-mediated control of stomatal aperture. *Curr Opin Plant Biol*., 154–162. https://doi.org/10.1016/j.pbi.2015.10.010.Mechanisms

Mustilli, A.-C., Merlot, S., Vavasseur, A., Fenzi, F., & Giraudat, J. (2002). Arabidopsis OST1 Protein Kinase Mediates the Regulation of Stomatal Aperture by Abscisic Acid and Acts Upstream of Reactive Oxygen Species Production. *The Plant Cell*, *14*(12), 3089 LP-3099. https://doi.org/10.1105/tpc.007906

Negi, J, Matsuda, O, Nagasawa, T, Oba, Y, Takahashi, H, Kawai-Yamada, M, Uchimiya, H, Hashimoto, M & Iba, K (2008). CO_2 regulator SLAC1 and its homologues are essential for anion homeostasis in plant cells. *Nature*, vol. 452, no. 7186, pp. 483-486. https://doi.org/10.1038/nature06720

Nilson, S. E., & Assmann, S. M. (2007). The Control of Transpiration. Insights from Arabidopsis. *Plant Physiology*, 1, *143*(January), 19–27. https://doi.org/10.1104/pp.106.093161

O'Connor, D. L. (2018). Live Confocal Imaging of Brachypodium Spikelet Meristems, b*io-protocol*, 8, 1–12. https://doi.org/10.21769/BioProtoc.3026

Ohashi-ito, K., & Bergmann, D. C. (2006). Arabidopsis FAMA Controls the Final Proliferation / Differentiation Switch during Stomatal Development. *The Plant Cell, 18*(October), 2493–2505. https://doi.org/10.1105/tpc.106.046136

Oosten, M. J. Van, Costa, A., Punzo, P., Landi, S., Ruggiero, A., Batelli, G., & Grillo, S. (2016). *Genetics of Drought Stress Tolerance in Crop Plants* (Vol. 2). https://doi.org/10.1007/978-3-319-32423-4

Pei Z-M, Murata Y, Benning G, Thomine S, KluÈsener B, Allen GJ, Grill E, Schroeder JI. (2000). Calcium channels activated by hydrogen peroxide mediate abscisic acid signalling in guard cells. *Nature* 406, 731±734.

Peterson, K. M., Rychel, A. L., & Torii, K. U. (2010). Out of the Mouths of Plants : The Molecular Basis of the Evolution and Diversity of Stomatal Development. *The Plant Cell*, *22*(February), 296–306. https://doi.org/10.1105/tpc.109.072777

Priest, H. D., Fox, S. E., Rowley, E. R., Murray, J. R., Michael, T. P., & Mockler, T. C. (2014). Analysis of Global Gene Expression in Brachypodium distachyon Reveals Extensive Network Plasticity in Response to Abiotic Stress, *9*(1). https://doi.org/10.1371/journal.pone.0087499

Qi, X., Han, S., Dang, J. H., & Garrick, J. M. (2017). Autocrine regulation of stomatal differentiation potential by EPF1 and ERECTA-LIKE1 ligand-receptor signaling. *eLife,* 1–21. https://doi.org/10.7554/eLife.24102

Raissig, M. T., Abrash, E., Bettadapur, A., Vogel, J. P., & Bergmann, D. C. (2016). Grasses use an alternatively wired bHLH transcription factor network to establish stomatal identity. *Proceedings of the National Academy of Sciences (PNAS)*, *113*(29), 8326 LP-8331. http://www.pnas.org/content/113/29/8326.abstract

Raissig, M. T., Matos, J. L., Gil, M. X. A., Kornfeld, A., Bettadapur, A., Abrash, E., & Bergmann, D. C. (2017). Mobile MUTE specifies subsidiary cells to build physiologically improved grass stomata, *Science 1218*(March), 1215–1218.

Raskin, I. and Ladyman, J.A.R. (1988) Isolation and characterization of a barley mutant with abscisic acid- insensitive stomata. *Planta*, 173, 73±78.

Rautengarten, C., Steinhauser, D., Bu, D., Stintzi, A., Schaller, A., & Kopka, J. (2005). Inferring Hypotheses on Functional Relationships of Genes: Analysis of the Arabidopsis thaliana Subtilase Gene Family. *PLOS 1*(4). https://doi.org/10.1371/journal.pcbi.0010040

Rowe, M. H., & Bergmann, D. C. (2010). Complex signals for simple cells: the expanding ranks of signals and receptors guiding stomatal development. *Current Opinion in Plant Biology*, *13*(5), 548–555. https://doi.org/https://doi.org/10.1016/j.pbi.2010.06.002

Rudall, P. J., Chen, E. D., & Cullen, E. (2017). Evolution and development of monocot stomata. *American Journal of Botany*, *104*(8), 1122–1141. https://doi.org/10.3732/ajb.1700086

Ruíz, M., Quemada, M., García, R. M., Carrillo, J. M., & Benavente, E. (2016). Use of thermographic imaging to screen for drought-tolerant genotypes in *Brachypodium distachyon*. *Crop and Pasture Science*, *67*(1), 99–108. https://doi.org/10.1071/CP15134

Ruszala EM, Beerling DJ, Franks PJ, Chater C, Casson SA, Gray JE, Hetherington AM (2011). Land plants acquired active stomatal control early in their evolutionary history. *Curr Biol*, 21:1030-1035.

Rychel, A. L., Peterson, K. M., & Torii, K. U. (2010). Plant twitter: ligands under 140 amino acids enforcing stomatal patterning. *J Plant Res*, 275–280. https://doi.org/10.1007/s10265-010-0330-9

Santrucek, J., Vrablova, M., Simkova, M., Hronkova, M., Drtinova, M., Kveton, J., Vrabl, D., Mackova, J., Wiesnerova, D., Neuwithova, J., Schreiber, L. (2014). Stomatal and pavement cell density linked to leaf internal CO 2 concentration. *Annals of Botany,* 114:191–202. https://doi.org/10.1093/aob/mcu095

Scavo, A. J., Sidhom, M., Rangel, F. J., Miaule, A., Emuka, C., Poomchongko, N, Ali, S., Rappe, W.J., Schroeder, J. I. (2018). Possible impacts of rising CO 2 on crop water use efficiency and food security. *California Agriculture 72*: 3(September), 155–158.

Schaller, A., Stintzi, A., & Graff, L. (2012). Subtilases – versatile tools for protein turnover, plant development, and interactions with the environment. *Physiologia Plantarum*, *145*(1), 52–66. https://doi.org/10.1111/j.1399-3054.2011.01529.x

Scholthof, K. G., Irigoyen, S., Catalan, P., & Mandadi, K. K. (2018). Brachypodium: A Monocot Grass Model Genus for Plant Biology. Plant Cell Adavanceshttps://doi.org/10.1105/tpc.18.00083

Shimada, T., & Sugano, S. S. (2011). Positive and negative peptide signals control stomatal density. *Cell*, 2081–2088. https://doi.org/10.1007/s00018-011-0685-7

Shpak, E.D., Berthiaume, C.T., Hill, E.J., and Torii, K.U. (2004). Synergistic interaction of three ERECTA-family receptor-like kinases controls Arabidopsis organ growth and flower development by promoting cell proliferation. *Development* 131: 1491–1501.

Somyong, S., Munkvold, J. D., Tanaka, J., Benscher, D., & Sorrells, M. E. (2011). Comparative genetic analysis of a wheat seed dormancy QTL with rice and Brachypodium identifies candidate genes for ABA perception and calcium signaling, 479–490. https://doi.org/10.1007/s10142-011-0219-2

Sugano, S. S., Shimada, T., Imai, Y., Okawa, K., Tamai, A., & Mori, M. (2010). Stomagen positively regulates stomatal density in Arabidopsis. *Nature*, *463*(7278), 241–244. https://doi.org/10.1038/nature08682

The Brachypodium Initiative (2010). Genome sequencing and analysis of the model grass Brachypodium distachyon. *Nature*, *463*, 763. http://dx.doi.org/10.1038/nature08747

Tian, W., Hou, C., Ren, Z., Pan, Y., Jia, J., Zhang, H., Bai, F., Zhang, P., Zhu, H., He, Y., Luo, S., Li, L., Luan, S. (2015). A molecular pathway for CO2 response in Arabidopsis guard cells. *Nature Communications*, *2*, 1–10. https://doi.org/10.1038/ncomms7057

Till BJ, Colbert T, Tompa R, Enns LC, Codomo CA, et al. (2003) High- throughput TILLING for functional genomics. *Methods In Molecular Biology* 236: 205–220.

Till BJ, Reynolds SH, Greene EA, Codomo CA, Enns LC, et al. (2003) Large- scale discovery of induced point mutations with high-throughput TILLING. *Genome research* 13: 524–53

Vatén, A., & Bergmann, D. C. (2012). Mechanisms of stomatal development: an evolutionary view. *EvoDevo*, 3:11, 1–9. http://www.evodevojournal.com/content/3/1/11

Vogel, J., & Bragg, J. (2009). Brachypodium distachyon, a New Model for the Triticeae. In C. Feuillet & G. J. Muehlhauer (Eds.), *Plant Genetics and Genomics: Crops and Models 7* (Genetics a, pp. 427–449). Sringer Science+Business Media. LLC. https://doi.org/10. l007/9780387-774893_l6. ©

Vogel, J., Brkljacic, J., Grotewold, E., Scholl, R., Mockler, T., & Garvin, D. F. (2011). Brachypodium as a model for the grasses: Today and the future. *Plant Physiology*. https://doi.org/10.1104/pp.111.179531

Vrablova, M., Vrabl, D.., Hronkova, M., Kubasek, J., & Santrucek, J. (2017). Stomatal function, density and pattern, and CO 2 assimilation in Arabidopsis thaliana tmm1 and sdd1-1 mutants. *Plant Biology*, *19*, 689–701. https://doi.org/10.1111/plb.12577

Wang, C., Hu, H., Qin, X., Zeise, B., Xu, D., Rappel, W., & Boron, W. F. (2016). Reconstitution of CO 2 Regulation of SLAC1 Anion Channel and Function of CO 2 -Permeable PIP2 ; 1 Aquaporin as CARBONIC ANHYDRASE4 Interactor. *The Plant Cell, 28*(February), 568–582. https://doi.org/10.1105/tpc.15.00637

Wang, Y., Darracq, O., Dalmais, M., Blondet, E., Oria, N., Bouvier, M., & Sibout, R. (2013). A TILLING Platform for Functional Genomics in Brachypodium distachyon. *PLOS*. https://doi.org/10.1371/journal.pone.0065503

Wang, Y., Holroyd, G., Hetherington, A. M., & Ng, C. K. (2004). Seeing `cool' and `hot': infrared thermography as a tool for non-invasive, high-throughput screening of Arabidopsis guard cell signaling mutants. *Journal of Experimental Botany*, *55*(400), 1187–1193. https://doi.org/10.1093/jxb/erh135

Wengier, D. L., Lampard, G. R., & Bergmann, D. C. (2018). Dissection of MAPK signaling specificity through protein engineering in a developmental context, *BMC Plant Biology*, 1–17.

Xue, S., Hu, H., Ries, A., Merilo, E., Kollist, H., & Schroeder, J. I. (2011). Central functions of bicarbonate in S-type anion channel activation and OST1 protein kinase in CO 2 signal transduction in guard cell. *The EMBO Journal*, *30*(8), 1645–1658. https://doi.org/10.1038/emboj.2011.68

Yang, J., Ordiz, M. I., Jaworski, J. G., & Beachy, R. N. (2011). Plant Physiology and Biochemistry Induced accumulation of cuticular waxes enhances drought tolerance in Arabidopsis by changes in development of stomata. *Plant Physiology et Biochemistry*, *49*(12), 1448–1455. https://doi.org/10.1016/j.plaphy.2011.09.006

Yang, M., & Sack, F. D. (1995). The too many mouths and four lips mutations affect stomatal production in Arabidopsis. *The Plant Cell*, *7*(12), 2227 LP-2239. https://doi.org/10.1105/tpc.7.12.2227

Young, J.J., Mehta, S., Israelsson, M., Godoski, J., Grill, E., and Schroeder, J.I. (2006). CO(2) signaling in guard cells: calcium sensitivity response modulation, a Ca(2+)-independent phase, and CO(2) insensitivity of the gca2 mutant. *Proc. Natl. Acad. Sci.* 103, 7506–7511.

Zhang, J., De-oliveira-Ceciliato, P., Takahashi, Y., Schulze, S., Dubeaux, G., Hauser, F., Azoulay-Shemer, T., Tõldsepp, K., Kollist, H., Rappel, W., Schroeder, J. I. (2018). Insights into the Molecular Mechanisms of CO_2-Mediated Regulation of Stomatal Movements. *Current Biology*, *28*(23), R1356–R1363. https://doi.org/10.1016/j.cub.2018.10.015

Zhang, J., Wang, N., Miao, Y., Hauser, F., Mccammon, J. A., & Rappel, W. (2018). Identification of SLAC1 anion channel residues required for CO 2 / bicarbonate sensing and regulation of stomatal movements, *115*(44). https://doi.org/10.1073/pnas.1807624115